Chaotic oscillations of viscoelastic microtubes conveying pulsatile fluid

Mergen H. Ghayesh [a], Hamed Farokhi [b], Ali Farajpour [a*]

[a] *School of Mechanical Engineering, University of Adelaide, South Australia 5005, Australia,*
Email: mergen.ghayesh@adelaide.edu.au (M.H. Ghayesh)
[*] *Corresponding author: Email: ali.farajpourouderji@adelaide.edu.au, Tel: +610478686072 (A. Farajpour)*

[b] *Department of Aeronautics, Imperial College London, London SW7 2AZ, UK*
Email: h.farokhi@imperial.ac.uk (H. Farokhi)

Abstract

As the first endeavor, the influence of a pulsatile flow on the large-amplitude bifurcation behaviour of viscoelastic microtubes subject to longitudinal pretention is studied with special consideration to chaos. The viscoelastic microtube is surrounded by a nonlinear spring bed. A modified size-dependent nonlinear tube model is developed based on a combination of the couple stress theory and the Euler-Bernoulli theory. Hamilton's principle, as an equation derivation technique, and Galerkin's procedure, as a discretisation technique, are used. Finally, the discretised differential equations of the pulsatile-fluid-conveying viscoelastic microscale tube are solved using a time-integration approach. It is investigated that how the bifurcation response for both motions along the axial and transverse axes is highly dependent of the mean value and the amplitude of the speed of the pulsatile flow.

Keywords: Microtubes; Bifurcation; Pulsatile flow; Nonlinear behaviour; Size effects

1. Introduction

In some microelectromechanical systems (MEMS) such as microfluidic devices [1] and integrated pressure sensors [2], the fluid and the solid building blocks of the system interact with each other at the microscale level. Increasing the level of knowledge of these interactions is of great importance in order to properly design and manufacture these valuable MEMS-based devices.

In recent years, some continuum-based models for microscale structures have been developed in the literature since these models pave the path for better understanding and formulating of the experimental results and Molecular Dynamics simulations. Nonetheless, the mechanical characteristics of small-scale structures such as microscale beams and plates as well as nanoscale beams and plates are size-dependent [3-7]. Applying theoretical models based on the classical continuum mechanics (CLCM) to these structures might be not sufficiently accurate to describe their mechanical and physical behaviours as these models are scale free, and thus cannot capture the effects of the small size. A number of modified theoretical models such as the nonlocal elasticity and the modified couple stress theory (MCST) have been employed recently so as to capture size effects on the mechanical response of small-scale structures. Generally, the nonlocal elasticity is applied to structures at the nanoscale level whereas the MCST is employed for microscale structures. In the present paper, the size effects are modelled within the context of the MCST.

A modified continuum model was proposed by Wang [8] for the vibration analysis of microscale tubes containing flowing fluid; he obtained the linear natural frequencies of the fluid-conveying microsystem using the differential quadrature method; he compared the frequencies obtained by the MCST-based model with those predicted by the CLCM, and found

that the CLCM underestimates the linear natural frequencies. The fluid-induced vibration of beams embedded in an elastic medium was also investigated by Kural and Özkaya [9]; they studied the effects of scale parameter, spring constant and the fluid velocity on the vibration of the elastic microsystem. Furthermore, Hosseini and Bahaadini [10] used a modified strain gradient continuum model to explore the linear stability of cantilever microscale tubes containing fluid flow with a constant speed. A nonlinear MCST-based mathematical framework was also proposed by Dehrouyeh-Semnani et al. [11] so as to study the large-amplitude vibration of a fluid-conveying pipe at microscale levels. The scale-dependent linear and nonlinear mechanics of carbon nanotubes conveying fluid flow of constant speed have been also studied in the literature mainly using the nonlocal continuum-based models [12-14]. Thermal effects on the forced linear and nonlinear vibrations of carbon nanotubes containing flowing fluid were also investigated on the basis of a nonlocal theoretical model by Askari and Esmailzadeh [15]; they reported that the speed of the flowing fluid and the temperature can be used to control the vibration of carbon nanotubes. Furthermore, Dehrouyeh-Semnani et al. [16] explored the influences of being microsized on the nonlinear stability of fluid-conveying pipes with geometric imperfections; they also investigated the influences of the flow velocity as well as the geometrical properties of the microsystem on the nonlinear stability. A nonlinear continuum model was also proposed by Setoodeh and Afrahim [17] in order to study the dynamic response of a functionally graded (FG) microscale tube containing fluid flow with the help of a strain gradient model. Moreover, Tang et al. [18] used the MCST to explore the influence of being microsized on the nonlinear fluid-induced vibration of curved microscale tubes. A non-classical beam model [19] and a nonlocal strain gradient model [20] for fluid-conveying micropipes as well as a flexoelectric couple stress model [21] for smart FG micropipes conveying fluid have been also developed.

In a practical situation, the speed of the flowing fluid in a MEMS device including fluid-structure interactions may not be *constant*; in general, it is a function of time. All of the above-stated valuable studies on the mechanical behaviour of fluid-conveying small-scale tubes are limited to *constant* fluid speeds. In this article, the bifurcation behaviour of viscoelastic microscale tubes containing fluid flow with *time-dependent* speed is constructed and analysed. The whole microsystem is assumed to be embedded in a nonlinear spring bed with two elastic coefficients. Two coupled time-dependent nonlinear differential equations are derived for the viscoelastic tube at microscale levels applying Hamilton's principle. Galerkin's technique and an integration scheme are then used in order to find a precise numerical solution for the derived equations. The effects of the mean value of the time-dependent fluid velocity as well as the amplitude of the variations of the microfluid velocity on the bifurcation behaviour of viscoelastic microscale tubes are explored, with special consideration to chaos.

2. Size-dependent continuum-based formulation and solution procedure

A viscoelastic microscale tube containing pulsatile flowing fluid is depicted in Fig. 1. As can be seen from the figure, the microtube is surrounded by a nonlinear elastic medium with two spring constants: 1) $k_1 \equiv$ the linear spring constant, and 2) $k_2 \equiv$ the nonlinear spring constant. It is also assumed that the viscoelastic microtube is subject to a longitudinal pretention (T_0). The internal and external radii of the microscale tube are denoted by R_i and R_o, respectively, while its length and cross-sectional area are denoted by L and A, respectively. Moreover, the material properties of the viscoelastic microscale tube are indicated by E, ν and c_{vis} which are the elasticity modulus, Poisson's ratio and the viscosity constant, respectively. To describe the influence of being microsized on the bifurcation behaviour, a

scale parameter (l) is also taken into account in the continuum-based formulation using the MCST.

The Kelvin-Voigt model is utilised to incorporate the effect of internal friction on the bifurcation behaviour. Using this model, the relation between the total axial stress (σ_{xx}) and the strain (ε_{xx}) can be expressed as

$$\sigma_{xx} = \sigma_{xx(el)} + \sigma_{xx(vis)}, \quad \text{with} \quad \begin{Bmatrix} \sigma_{xx(el)} \\ \sigma_{xx(vis)} \end{Bmatrix} = \begin{Bmatrix} E\varepsilon_{xx} \\ c_{vis}\dfrac{\partial \varepsilon_{xx}}{\partial t} \end{Bmatrix}. \tag{1}$$

Here $\sigma_{xx(el)}$ and $\sigma_{xx(vis)}$ are respectively the elastic and viscous axial stresses. Let us denote the axial displacement and the transverse deflection of the mid-plane of the viscoelastic microscale tube by *u* and *v*, respectively. The nonlinear strain component of an Euler-Bernoulli microtube can be written as

$$\varepsilon_{xx}(x,z,t) = \left\{ \left[\frac{\partial u(x,t)}{\partial x} + 1 \right]^2 + \left[\frac{\partial v(x,t)}{\partial x} \right]^2 \right\}^{\frac{1}{2}} - 1 - z\frac{\partial \psi(x,t)}{\partial x}, \tag{2}$$

where $\psi(x,t)$ represents the rotation of the cross section of the microtube. Similarly, applying the Kelvin-Voigt model to the deviatoric couple stress tensor (DCST), one obtains

$$\begin{Bmatrix} m_{xy} \\ m_{yz} \end{Bmatrix} = \begin{Bmatrix} m_{xy(el)} + m_{xy(vis)} \\ m_{yz(el)} + m_{yz(vis)} \end{Bmatrix}, \tag{3}$$

where m_{xy} and m_{yz} are the symmetric components of the DCST; also, $m_{ij(el)}$ and $m_{ij(vis)}$ are respectively the elastic and viscous parts of the symmetric DCST which are given by

$$\begin{Bmatrix} m_{xy(el)} \\ m_{yz(el)} \end{Bmatrix} = \begin{Bmatrix} \tilde{E}\chi_{xy} \\ \tilde{E}\chi_{yz} \end{Bmatrix}, \quad \begin{Bmatrix} m_{xy(vis)} \\ m_{yz(vis)} \end{Bmatrix} = \begin{Bmatrix} \tilde{c}_{vis}\dfrac{\partial \chi_{xy}}{\partial t} \\ \tilde{c}_{vis}\dfrac{\partial \chi_{yz}}{\partial t} \end{Bmatrix}, \tag{4}$$

where

$$\tilde{E} = \frac{El^2}{1+\nu}, \quad \tilde{c}_{vis} = \frac{c_{vis}l^2}{1+\nu}. \tag{5}$$

In the above relation (i.e. Eq. (5)), $\left[\chi_{ij}\right]$ describes the symmetric rotation gradient of the microtube which is obtained as

$$\begin{Bmatrix} \chi_{xy} \\ \chi_{yz} \end{Bmatrix} = -\begin{Bmatrix} \dfrac{1}{4}\dfrac{\partial}{\partial x}\left(\sin\psi + \dfrac{\partial v}{\partial x}\right) + \dfrac{z}{4}\dfrac{\partial^2 \cos\psi}{\partial x^2} \\ \dfrac{1}{4}\dfrac{\partial \cos\psi}{\partial x} \end{Bmatrix}. \tag{6}$$

The variation of the elastic energy due to the longitudinal pretention as well as the elastic axial stress and the elastic symmetric DCST can be expressed as

$$\begin{aligned} \delta U_{el} &= \int_0^L \int_A T_0 \delta\varepsilon_{xx}\, \mathrm{d}A\mathrm{d}x + \int_0^L \int_A \sigma_{xx(el)}\delta\varepsilon_{xx}\, \mathrm{d}A\mathrm{d}x \\ &+2\int_0^L \int_A \left(m_{xy(el)}\delta\chi_{xy} + m_{yz(el)}\delta\chi_{yz}\right)\mathrm{d}A\mathrm{d}x. \end{aligned} \tag{7}$$

In the same way, the work performed by the viscous stress and the viscous symmetric DCST are obtained as

$$\delta W_{vis} = -\int_0^L \int_A \left[\sigma_{xx(vis)}\delta\varepsilon_{xx} + 2\left(m_{xy(vis)}\delta\chi_{xy} + m_{yz(vis)}\delta\chi_{yz}\right)\right]\mathrm{d}A\mathrm{d}x. \tag{8}$$

The motion energy of a microscale tube containing fluid flow with a time-dependent speed can be formulated as

$$T_{me}=\frac{1}{2}\int_0^L\left\{m\left(\frac{\partial u}{\partial t}\right)^2+M\left[\frac{\partial u}{\partial t}+U(t)\left(1+\frac{\partial u}{\partial x}\right)\right]^2\right\}dx$$
$$+\frac{1}{2}\int_0^L\left\{m\left(\frac{\partial v}{\partial t}\right)^2+M\left[\frac{\partial v}{\partial t}+U(t)\frac{\partial v}{\partial x}\right]^2\right\}dx. \tag{9}$$

Here T_{me}, $U(t)$, m and M are the motion energy, the fluid speed, the mass of the microtube and the microfluid per unit length, respectively. The subscript "*me*" stands for the motion energy. The energy variation induced by the nonlinear elastic medium can be written as

$$\delta U_{em}=\int_0^L\left(k_1v+k_2v^3\right)\delta v\,\mathrm{d}x, \tag{10}$$

in which the subscript "*em*" stands for the elastic medium. The above-mentioned energy and work terms are related to each other by

$$\int_{t_1}^{t_2}\left(\delta T_{me}-\delta U_{el}-\delta U_{em}+\delta W_{vis}\right)\mathrm{d}t=0. \tag{11}$$

Substituting Eqs. (7)-(10) into Eq. (11) and integrating by parts, one obtains the following coupled time-dependent nonlinear differential equations for pulsatile-fluid-conveying viscoelastic tubes at microscale levels

$$\frac{\partial^2u}{\partial t^2}+\beta\frac{\partial U}{\partial t}+\beta\frac{\partial U}{\partial t}\frac{\partial u}{\partial x}+\left(\beta U^2-\frac{EA}{M+m}\right)\frac{\partial^2u}{\partial x^2}+2\beta U\frac{\partial^2u}{\partial x\partial t}$$
$$-\left(\frac{EA}{m+M}\right)\frac{\partial v}{\partial x}\frac{\partial^2v}{\partial x^2}-\frac{1}{m+M}\left(EI+\frac{\tilde{E}A}{4}\right)\left(\frac{\partial^2v}{\partial x^2}\frac{\partial^3v}{\partial x^3}+\frac{\partial v}{\partial x}\frac{\partial^4v}{\partial x^4}\right)$$
$$-\left(\frac{c_{vis}A}{m+M}\right)\left(\frac{\partial^3u}{\partial t\partial x^2}+\frac{\partial^2v}{\partial x^2}\frac{\partial^2v}{\partial t\partial x}+\frac{\partial v}{\partial x}\frac{\partial^3v}{\partial t\partial x^2}\right)$$
$$-\frac{1}{m+M}\left(c_{vis}I+\frac{\tilde{c}_{vis}A}{4}\right)\left(\frac{\partial^2v}{\partial x^2}\frac{\partial^4v}{\partial t\partial x^3}+\frac{\partial v}{\partial x}\frac{\partial^5v}{\partial t\partial x^4}\right)=0, \tag{12}$$

$$
\begin{aligned}
&\frac{\partial^2 v}{\partial t^2}+\beta\frac{\partial U}{\partial t}\frac{\partial v}{\partial x}+\left(\beta U^2-\frac{T_0}{m+M}\right)\frac{\partial^2 v}{\partial x^2}+2\beta U\frac{\partial^2 v}{\partial x\partial t}\\
&+\left(\frac{EI}{m+M}\right)\frac{\partial^4 v}{\partial x^4}-\left(\frac{EA}{m+M}\right)\left[\frac{3}{2}\left(\frac{\partial v}{\partial x}\right)^2\frac{\partial^2 v}{\partial x^2}+\frac{\partial^2 v}{\partial x^2}\frac{\partial u}{\partial x}+\frac{\partial v}{\partial x}\frac{\partial^2 u}{\partial x^2}\right]\\
&-\left(\frac{EI}{m+M}\right)\left[2\left(\frac{\partial^2 v}{\partial x^2}\right)^3+2\left(\frac{\partial v}{\partial x}\right)^2\frac{\partial^4 v}{\partial x^4}+8\frac{\partial v}{\partial x}\frac{\partial^2 v}{\partial x^2}\frac{\partial^3 v}{\partial x^3}+3\frac{\partial^3 u}{\partial x^3}\frac{\partial^2 v}{\partial x^2}\right.\\
&\left.+\frac{\partial^4 u}{\partial x^4}\frac{\partial v}{\partial x}+4\frac{\partial^2 u}{\partial x^2}\frac{\partial^3 v}{\partial x^3}+2\frac{\partial u}{\partial x}\frac{\partial^4 v}{\partial x^4}\right]-\frac{\tilde{E}I}{8(m+M)}\left[3\frac{\partial^2 v}{\partial x^2}\left(\frac{\partial^3 v}{\partial x^3}\right)^2\right.\\
&\left.+10\frac{\partial v}{\partial x}\frac{\partial^3 v}{\partial x^3}\frac{\partial^4 v}{\partial x^4}+\frac{\partial^6 v}{\partial x^6}\left(\frac{\partial v}{\partial x}\right)^2+6\frac{\partial v}{\partial x}\frac{\partial^2 v}{\partial x^2}\frac{\partial^5 v}{\partial x^5}+4\frac{\partial^4 v}{\partial x^4}\left(\frac{\partial^2 v}{\partial x^2}\right)^2\right]\\
&+\frac{\tilde{E}A}{8(m+M)}\left[4\frac{\partial^4 v}{\partial x^4}-6\frac{\partial^3 u}{\partial x^3}\frac{\partial^2 v}{\partial x^2}-4\frac{\partial u}{\partial x}\frac{\partial^4 v}{\partial x^4}-5\left(\frac{\partial^2 v}{\partial x^2}\right)^3-20\frac{\partial v}{\partial x}\frac{\partial^2 v}{\partial x^2}\frac{\partial^3 v}{\partial x^3}\right.\\
&\left.-2\frac{\partial^4 u}{\partial x^4}\frac{\partial v}{\partial x}-5\frac{\partial^4 v}{\partial x^4}\left(\frac{\partial v}{\partial x}\right)^2-8\frac{\partial^2 u}{\partial x^2}\frac{\partial^3 v}{\partial x^3}\right]+\left(\frac{k_1}{m+M}\right)v+\left(\frac{k_2}{m+M}\right)v^3\\
&-\frac{c_{vis}A}{(m+M)}\left[\frac{\partial^3 v}{\partial t\partial x^2}\left(\frac{\partial v}{\partial x}\right)^2+\frac{\partial^3 u}{\partial t\partial x^2}\frac{\partial v}{\partial x}+2\frac{\partial^2 v}{\partial t\partial x}\frac{\partial^2 v}{\partial x^2}\frac{\partial v}{\partial x}+\frac{\partial^2 u}{\partial t\partial x}\frac{\partial^2 v}{\partial x^2}\right]\\
&+\frac{c_{vis}I}{(m+M)}\left[\frac{\partial^5 v}{\partial t\partial x^4}-\frac{\partial^4 u}{\partial x^4}\frac{\partial^2 v}{\partial t\partial x}-\frac{\partial^5 u}{\partial t\partial x^4}\frac{\partial v}{\partial x}-3\frac{\partial^2 v}{\partial x^2}\frac{\partial^4 u}{\partial t\partial x^3}-6\frac{\partial^2 v}{\partial x^2}\frac{\partial^3 v}{\partial x^3}\frac{\partial^2 v}{\partial t\partial x}\right.\\
&-3\frac{\partial^3 u}{\partial x^3}\frac{\partial^3 v}{\partial t\partial x^2}-3\frac{\partial^3 u}{\partial t\partial x^2}\frac{\partial^3 v}{\partial x^3}-2\frac{\partial u}{\partial x}\frac{\partial^5 v}{\partial t\partial x^4}-4\frac{\partial^2 u}{\partial x^2}\frac{\partial^4 v}{\partial t\partial x^3}-6\frac{\partial^3 v}{\partial t\partial x^2}\frac{\partial^3 v}{\partial x^3}\frac{\partial v}{\partial x}\\
&\left.-\frac{\partial^2 u}{\partial t\partial x}\frac{\partial^4 v}{\partial x^4}-2\frac{\partial^5 v}{\partial t\partial x^4}\left(\frac{\partial v}{\partial x}\right)^2-8\frac{\partial^2 v}{\partial x^2}\frac{\partial v}{\partial x}\frac{\partial^4 v}{\partial t\partial x^3}-6\frac{\partial^3 v}{\partial t\partial x^2}\left(\frac{\partial^2 v}{\partial x^2}\right)^2-2\frac{\partial v}{\partial x}\frac{\partial^2 v}{\partial t\partial x}\frac{\partial^4 v}{\partial x^4}\right]\\
&+\frac{\tilde{c}_{vis}A}{8(m+M)}\left[4\frac{\partial^5 v}{\partial t\partial x^4}-2\frac{\partial^5 u}{\partial t\partial x^4}\frac{\partial v}{\partial x}-17\frac{\partial^2 v}{\partial t\partial x}\frac{\partial^3 v}{\partial x^3}\frac{\partial^2 v}{\partial x^2}-6\frac{\partial^4 u}{\partial t\partial x^3}\frac{\partial^2 v}{\partial x^2}-15\frac{\partial v}{\partial x}\frac{\partial^3 v}{\partial t\partial x^2}\frac{\partial^3 v}{\partial x^3}\right.\\
&-5\frac{\partial^2 v}{\partial t\partial x}\frac{\partial v}{\partial x}\frac{\partial^4 v}{\partial x^4}-8\frac{\partial^2 u}{\partial x^2}\frac{\partial^4 v}{\partial t\partial x^3}-6\frac{\partial^3 u}{\partial x^3}\frac{\partial^3 v}{\partial t\partial x^2}-2\frac{\partial^4 v}{\partial x^4}\frac{\partial^2 u}{\partial t\partial x}-6\frac{\partial^3 u}{\partial t\partial x^2}\frac{\partial^3 v}{\partial x^3}\\
&\left.-20\frac{\partial v}{\partial x}\frac{\partial^2 v}{\partial x^2}\frac{\partial^4 v}{\partial t\partial x^3}-2\frac{\partial^2 v}{\partial t\partial x}\frac{\partial^4 u}{\partial x^4}-4\frac{\partial^5 v}{\partial t\partial x^4}\frac{\partial u}{\partial x}-5\left(\frac{\partial v}{\partial x}\right)^2\frac{\partial^5 v}{\partial t\partial x^4}-16\frac{\partial^3 v}{\partial t\partial x^2}\left(\frac{\partial^2 v}{\partial x^2}\right)^2\right]\\
&-\frac{\tilde{c}_{vis}I}{8(m+M)}\left[\frac{\partial^2 v}{\partial t\partial x}\frac{\partial^5 v}{\partial x^5}\frac{\partial^2 v}{\partial x^2}+\frac{\partial^7 v}{\partial t\partial x^6}\left(\frac{\partial v}{\partial x}\right)^2+5\frac{\partial v}{\partial x}\frac{\partial^5 v}{\partial x^5}\frac{\partial^3 v}{\partial t\partial x^2}+6\frac{\partial^2 v}{\partial x^2}\frac{\partial^3 v}{\partial x^3}\frac{\partial^4 v}{\partial t\partial x^3}\right.\\
&+\frac{\partial v}{\partial x}\frac{\partial^2 v}{\partial t\partial x}\frac{\partial^6 v}{\partial x^6}+4\frac{\partial^5 v}{\partial t\partial x^4}\left(\frac{\partial^2 v}{\partial x^2}\right)^2+4\frac{\partial^2 v}{\partial x^2}\frac{\partial^3 v}{\partial t\partial x^2}\frac{\partial^4 v}{\partial x^4}+10\frac{\partial v}{\partial x}\frac{\partial^3 v}{\partial x^3}\frac{\partial^5 v}{\partial t\partial x^4}\\
&\left.+10\frac{\partial^4 v}{\partial t\partial x^3}\frac{\partial v}{\partial x}\frac{\partial^4 v}{\partial x^4}+6\frac{\partial^6 v}{\partial t\partial x^5}\frac{\partial v}{\partial x}\frac{\partial^2 v}{\partial x^2}\right]=0,
\end{aligned}
\tag{13}
$$

in which $\beta = M/(M+m)$. Now let us consider the following time-dependent profile for the fluid velocity

$$U = U_0 + U_1 \cos(\omega_f t), \tag{14}$$

where U_0 and U_f indicate the mean value of the microfluid velocity and the amplitude of the variations of the microfluid velocity, respectively; ω_f represents the frequency of the flow pulsation. In order to rewrite Eqs. (12) and (13) in a dimensionless form, the following parameters are given for the viscoelastic microsystem

$$\begin{aligned}
&\alpha = \frac{x}{L},\ \zeta = \frac{u}{2R_o},\ \eta = \frac{v}{2R_o},\ \gamma = \frac{L}{2R_o},\ \tau = \frac{t}{L^2}\sqrt{\frac{EI}{(M+m)}},\ \Gamma = \frac{T_0 L^2}{EI},\\
&\bar{c}_{vis} = \frac{c_{vis}}{E}\sqrt{\frac{EI}{(M+m)L^4}},\ \Xi_g = \frac{AL^2}{I},\ \bar{\mu} = \frac{Al^2}{2(1+\nu)I},\ \varpi_f = \omega_f L^2\sqrt{\frac{M+m}{EI}},\\
&u_f = \sqrt{\frac{M}{EI}}UL,\ u_{f0} = \sqrt{\frac{M}{EI}}U_0 L,\ u_{f1} = \sqrt{\frac{M}{EI}}U_1 L,\ K_1 = \frac{k_1 L^4}{EI},\ K_2 = \frac{4k_2 L^4 R_o^2}{EI}.
\end{aligned} \tag{15}$$

Substituting Eq. (14) into eqs. (12) and (13), and then using Eq. (15), we have

$$\begin{aligned}
&\frac{\partial^2\zeta}{\partial\tau^2} - \gamma\sqrt{\beta}u_{f1}\varpi_f \sin(\varpi_f\tau) - \sqrt{\beta}u_{f1}\varpi_f \sin(\varpi_f\tau)\frac{\partial\zeta}{\partial\alpha}\\
&+\left\{\left[u_{f0} + u_{f1}\cos(\varpi_f\tau)\right]^2 - \Xi_g\right\}\frac{\partial^2\zeta}{\partial\alpha^2} + 2\sqrt{\beta}\left[u_{f0} + u_{f1}\cos(\varpi_f\tau)\right]\frac{\partial^2\zeta}{\partial\alpha\partial\tau} - \frac{\Xi_g}{\gamma}\frac{\partial\eta}{\partial\alpha}\frac{\partial^2\eta}{\partial\alpha^2}\\
&-\frac{1}{\gamma}\left(1+\frac{1}{2}\bar{\mu}\right)\left(\frac{\partial^2\eta}{\partial\alpha^2}\frac{\partial^3\eta}{\partial\alpha^3} + \frac{\partial\eta}{\partial\alpha}\frac{\partial^4\eta}{\partial\alpha^4}\right) - \frac{\Xi_g\bar{c}_{vis}}{\gamma}\left(\gamma\frac{\partial^3\zeta}{\partial\tau\partial\alpha^2} + \frac{\partial^2\eta}{\partial\alpha^2}\frac{\partial^2\eta}{\partial\tau\partial\alpha} + \frac{\partial\eta}{\partial\alpha}\frac{\partial^3\eta}{\partial\tau\partial\alpha^2}\right)\\
&-\frac{\bar{c}_{vis}}{\gamma}\left(1+\frac{1}{2}\bar{\mu}\right)\left(\frac{\partial^4\eta}{\partial\tau\partial\alpha^3}\frac{\partial^2\eta}{\partial\alpha^2} + \frac{\partial^5\eta}{\partial\tau\partial\alpha^4}\frac{\partial\eta}{\partial\alpha}\right) = 0,
\end{aligned} \tag{16}$$

$$\begin{aligned}
&\frac{\partial^2\eta}{\partial\tau^2} - \sqrt{\beta}\varpi_f u_{f1}\sin(\varpi_f\tau)\frac{\partial\eta}{\partial\alpha} + \left\{\left[u_{f0} + u_{f1}\cos(\varpi_f\tau)\right]^2 - \Gamma\right\}\frac{\partial^2\eta}{\partial\alpha^2}\\
&+2\sqrt{\beta}\left[u_{f0} + u_{f1}\cos(\varpi_f\tau)\right]\frac{\partial^2\eta}{\partial\tau\partial\alpha} + (1+\bar{\mu})\frac{\partial^4\eta}{\partial\alpha^4}\\
&-\frac{\Xi_g}{\gamma}\left[\frac{3}{2\gamma}\frac{\partial^2\eta}{\partial\alpha^2}\left(\frac{\partial\eta}{\partial\alpha}\right)^2 + \frac{\partial\eta}{\partial\alpha}\frac{\partial^2\zeta}{\partial\alpha^2} + \frac{\partial^2\eta}{\partial\alpha^2}\frac{\partial\zeta}{\partial\alpha}\right] + K_1\eta + K_2\eta^3
\end{aligned}$$

$$-\frac{1}{\gamma}\left\{4\frac{\partial^3\eta}{\partial\alpha^3}\frac{\partial^2\zeta}{\partial\alpha^2}+3\frac{\partial^2\eta}{\partial\alpha^2}\frac{\partial^3\zeta}{\partial\alpha^3}+\frac{\partial\eta}{\partial\alpha}\frac{\partial^4\zeta}{\partial\alpha^4}+2\frac{\partial^4\eta}{\partial\alpha^4}\frac{\partial\zeta}{\partial\alpha}\right.$$
$$\left.+\frac{1}{\gamma}\left[2\left(\frac{\partial^2\eta}{\partial\alpha^2}\right)^3+2\left(\frac{\partial\eta}{\partial\alpha}\right)^2\frac{\partial^4\eta}{\partial\alpha^4}+8\frac{\partial\eta}{\partial\alpha}\frac{\partial^2\eta}{\partial\alpha^2}\frac{\partial^3\eta}{\partial\alpha^3}\right]\right\}$$
$$-\frac{1}{4}\frac{\bar{\mu}}{\gamma}\left\{6\frac{\partial^2\eta}{\partial\alpha^2}\frac{\partial^3\zeta}{\partial\alpha^3}+2\frac{\partial\eta}{\partial\alpha}\frac{\partial^4\zeta}{\partial\alpha^4}+4\frac{\partial^4\eta}{\partial\alpha^4}\frac{\partial\zeta}{\partial\alpha}+8\frac{\partial^3\eta}{\partial\alpha^3}\frac{\partial^2\zeta}{\partial\alpha^2}\right.$$
$$\left.+\frac{1}{\gamma}\left[5\left(\frac{\partial^2\eta}{\partial\alpha^2}\right)^3+5\left(\frac{\partial\eta}{\partial\alpha}\right)^2\frac{\partial^4\eta}{\partial\alpha^4}+20\frac{\partial\eta}{\partial\alpha}\frac{\partial^2\eta}{\partial\alpha^2}\frac{\partial^3\eta}{\partial\alpha^3}\right]\right\}$$
$$-\frac{1}{4}\frac{\bar{\mu}}{\Xi_g\gamma^2}\left[3\left(\frac{\partial^3\eta}{\partial\alpha^3}\right)^2\frac{\partial^2\eta}{\partial\alpha^2}+6\frac{\partial^5\eta}{\partial\alpha^5}\frac{\partial\eta}{\partial\alpha}\frac{\partial^2\eta}{\partial\alpha^2}\right.$$
$$\left.+10\frac{\partial^4\eta}{\partial\alpha^4}\frac{\partial\eta}{\partial\alpha}\frac{\partial^3\eta}{\partial\alpha^3}+\frac{\partial^6\eta}{\partial\alpha^6}\left(\frac{\partial\eta}{\partial\alpha}\right)^2+4\frac{\partial^4\eta}{\partial\alpha^4}\left(\frac{\partial^2\eta}{\partial\alpha^2}\right)^2\right]$$
$$-\frac{\bar{c}_{vis}\Xi_g}{\gamma}\left[\frac{1}{\gamma}\left(\frac{\partial^3\eta}{\partial\tau\partial\alpha^2}\left(\frac{\partial\eta}{\partial\alpha}\right)^2+2\frac{\partial^2\eta}{\partial\alpha^2}\frac{\partial\eta}{\partial\alpha}\frac{\partial^2\eta}{\partial\tau\partial\alpha}\right)+\frac{\partial\eta}{\partial\alpha}\frac{\partial^3\zeta}{\partial\tau\partial\alpha^2}+\frac{\partial^2\eta}{\partial\alpha^2}\frac{\partial^2\zeta}{\partial\tau\partial\alpha}\right]$$
$$+\bar{c}_{vis}\left[\frac{\partial^5\eta}{\partial\tau\partial\alpha^4}-\frac{1}{\gamma}\left(\frac{\partial^4\zeta}{\partial\alpha^4}\frac{\partial^2\eta}{\partial\tau\partial\alpha}+\frac{\partial\eta}{\partial\alpha}\frac{\partial^5\zeta}{\partial\tau\partial\alpha^4}+\frac{\partial^4\eta}{\partial\alpha^4}\frac{\partial^2\zeta}{\partial\tau\partial\alpha}+2\frac{\partial^5\eta}{\partial\tau\partial\alpha^4}\frac{\partial\zeta}{\partial\alpha}\right.\right.$$
$$\left.+3\frac{\partial^2\eta}{\partial\alpha^2}\frac{\partial^4\zeta}{\partial\tau\partial\alpha^3}+4\frac{\partial^4\eta}{\partial\tau\partial\alpha^3}\frac{\partial^2\zeta}{\partial\alpha^2}+3\frac{\partial^3\zeta}{\partial\alpha^3}\frac{\partial^3\eta}{\partial\tau\partial\alpha^2}+3\frac{\partial^3\eta}{\partial\alpha^3}\frac{\partial^3\zeta}{\partial\tau\partial\alpha^2}\right)$$
$$-\frac{1}{\gamma^2}\left(6\frac{\partial^3\eta}{\partial\alpha^3}\frac{\partial^2\eta}{\partial\alpha^2}\frac{\partial^2\eta}{\partial\tau\partial\alpha}+8\frac{\partial^2\eta}{\partial\alpha^2}\frac{\partial^4\eta}{\partial\tau\partial\alpha^3}\frac{\partial\eta}{\partial\alpha}+6\frac{\partial\eta}{\partial\alpha}\frac{\partial^3\eta}{\partial\tau\partial\alpha^2}\frac{\partial^3\eta}{\partial\alpha^3}\right.$$
$$\left.\left.+2\frac{\partial^5\eta}{\partial\tau\partial\alpha^4}\left(\frac{\partial\eta}{\partial\alpha}\right)^2+6\left(\frac{\partial^2\eta}{\partial\alpha^2}\right)^2\frac{\partial^3\eta}{\partial\tau\partial\alpha^2}+2\frac{\partial^4\eta}{\partial\alpha^4}\frac{\partial^2\eta}{\partial\tau\partial\alpha}\frac{\partial\eta}{\partial\alpha}\right)\right]$$
$$+\frac{\bar{\mu}\bar{c}_{vis}}{4}\left[4\frac{\partial^5\eta}{\partial\tau\partial\alpha^4}-\frac{1}{\gamma}\left(2\frac{\partial^5\zeta}{\partial\tau\partial\alpha^4}\frac{\partial\eta}{\partial\alpha}+2\frac{\partial^4\zeta}{\partial\alpha^4}\frac{\partial^2\eta}{\partial\tau\partial\alpha}+6\frac{\partial^4\zeta}{\partial\tau\partial\alpha^3}\frac{\partial^2\eta}{\partial\alpha^2}+6\frac{\partial^3\zeta}{\partial\alpha^3}\frac{\partial^3\nu}{\partial\tau\partial\alpha^2}\right.\right.$$
$$\left.+6\frac{\partial^3\eta}{\partial\alpha^3}\frac{\partial^3\zeta}{\partial\tau\partial\alpha^2}+2\frac{\partial^4\eta}{\partial\alpha^4}\frac{\partial^2\zeta}{\partial\tau\partial\alpha}+4\frac{\partial^5\eta}{\partial\tau\partial\alpha^4}\frac{\partial\zeta}{\partial\alpha}+8\frac{\partial^4\eta}{\partial\tau\partial\alpha^3}\frac{\partial^2\zeta}{\partial\alpha^2}\right)$$
$$-\frac{1}{\gamma^2}\left(17\frac{\partial^2\eta}{\partial\tau\partial\alpha}\frac{\partial^2\eta}{\partial\alpha^2}\frac{\partial^3\eta}{\partial\alpha^3}+15\frac{\partial\eta}{\partial\alpha}\frac{\partial^3\eta}{\partial\tau\partial\alpha^2}\frac{\partial^3\eta}{\partial\alpha^3}+20\frac{\partial\eta}{\partial\alpha}\frac{\partial^2\eta}{\partial\alpha^2}\frac{\partial^4\eta}{\partial\tau\partial\alpha^3}\right.$$
$$\left.\left.+5\frac{\partial^5\eta}{\partial\tau\partial\alpha^4}\left(\frac{\partial\eta}{\partial\alpha}\right)^2+16\left(\frac{\partial^2\eta}{\partial\alpha^2}\right)^2\frac{\partial^3\eta}{\partial\tau\partial\alpha^2}+5\frac{\partial^4\eta}{\partial\alpha^4}\frac{\partial\eta}{\partial\alpha}\frac{\partial^2\eta}{\partial\tau\partial\alpha}\right)\right]$$

$$-\frac{\overline{\mu}\overline{c}_{vis}}{4\Xi_g\gamma^2}\left[\frac{\partial^5\eta}{\partial\alpha^5}\frac{\partial^2\eta}{\partial\tau\partial\alpha}\frac{\partial^2\eta}{\partial\alpha^2}+5\frac{\partial^3\eta}{\partial\tau\partial\alpha^2}\frac{\partial\eta}{\partial\alpha}\frac{\partial^5\eta}{\partial\alpha^5}+6\frac{\partial^6\eta}{\partial\tau\partial\alpha^5}\frac{\partial\eta}{\partial\alpha}\frac{\partial^2\eta}{\partial\alpha^2}+\frac{\partial^7\eta}{\partial\tau\partial\alpha^6}\left(\frac{\partial\eta}{\partial\alpha}\right)^2\right.$$
$$+\frac{\partial\eta}{\partial\alpha}\frac{\partial^2\eta}{\partial\tau\partial\alpha}\frac{\partial^6\eta}{\partial\alpha^6}+6\frac{\partial^3\eta}{\partial\alpha^3}\frac{\partial^2\eta}{\partial\alpha^2}\frac{\partial^4\eta}{\partial\tau\partial\alpha^3}+4\frac{\partial^3\eta}{\partial\tau\partial\alpha^2}\frac{\partial^2\eta}{\partial\alpha^2}\frac{\partial^4\eta}{\partial\alpha^4} \tag{17}$$
$$\left.+4\frac{\partial^5\eta}{\partial\tau\partial\alpha^4}\left(\frac{\partial^2\eta}{\partial\alpha^2}\right)^2+10\frac{\partial^4\eta}{\partial\alpha^4}\frac{\partial^4\eta}{\partial\tau\partial\alpha^3}\frac{\partial\eta}{\partial\alpha}+10\frac{\partial^3\eta}{\partial\alpha^3}\frac{\partial\eta}{\partial\alpha}\frac{\partial^5\eta}{\partial\tau\partial\alpha^4}\right]=0.$$

To accurately approximate the axial displacement and the transverse deflection of the pulsatile fluid-conveying viscoelastic microtube, the following expressions are used

$$\begin{Bmatrix}\eta(\alpha,\tau)\\ \zeta(\alpha,\tau)\end{Bmatrix}=\begin{Bmatrix}\sum_{m=1}^{N_v}q_m(\tau)\tilde{\eta}_m(\alpha)\\ \sum_{m=1}^{N_u}r_m(\tau)\tilde{\zeta}_m(\alpha)\end{Bmatrix}, \tag{18}$$

in which (q_m, r_m) and ($\tilde{\eta}_m$, $\tilde{\zeta}_m$) indicate the *m*th generalised coordinates and shape functions of the microtube, respectively. Inserting Eq. (18) into Eqs. (16) and (17), and then employing Galerkin's approach, one can obtain the following equations

$$\sum_{j=1}^{N_u}\left(\int_0^1\tilde{\zeta}_i\tilde{\zeta}_j d\alpha\right)\ddot{r}_j-\gamma\sqrt{\beta}u_{f1}\varpi_f\sin(\varpi_f\tau)\int_0^1\tilde{\zeta}_i d\alpha-\sqrt{\beta}u_{f1}\varpi_f\sin(\varpi_f\tau)\sum_{j=1}^{N_u}\left(\int_0^1\tilde{\zeta}_i\tilde{\zeta}_j' d\alpha\right)r_j$$
$$+\left\{\left[u_{f0}+u_{f1}\cos(\varpi_f\tau)\right]^2-\Xi_g\right\}\sum_{j=1}^{N_u}\left(\int_0^1\tilde{\zeta}_i\tilde{\zeta}_j'' d\alpha\right)r_j$$
$$+2\sqrt{\beta}\left[u_{f0}+u_{f1}\cos(\varpi_f\tau)\right]\sum_{j=1}^{N_u}\left(\int_0^1\tilde{\zeta}_i\tilde{\zeta}_j' d\alpha\right)\dot{r}_j-\frac{\Xi_g}{\gamma}\sum_{j=1}^{N_v}\sum_{k=1}^{N_v}\left(\int_0^1\tilde{\zeta}_i\tilde{\eta}_j'\tilde{\eta}_k'' d\alpha\right)q_jq_k$$
$$-\frac{1}{\gamma}\left(1+\frac{1}{2}\overline{\mu}\right)\sum_{j=1}^{N_v}\sum_{k=1}^{N_v}\left(\int_0^1\tilde{\zeta}_i\tilde{\eta}_k'''\tilde{\eta}_j''\,d\alpha+\int_0^1\tilde{\zeta}_i\tilde{\eta}_k''''\tilde{\eta}_j'\,d\alpha\right)q_jq_k \tag{19}$$
$$-\frac{\Xi_g\overline{c}_{vis}}{\gamma}\left[\gamma\sum_{j=1}^{N_u}\left(\int_0^1\tilde{\zeta}_i\tilde{\zeta}_j'' d\alpha\right)\dot{r}_j+\sum_{j=1}^{N_v}\sum_{k=1}^{N_v}\left(\int_0^1\tilde{\zeta}_i\tilde{\eta}_j'\tilde{\eta}_k''\,d\alpha\right)\left(\dot{q}_jq_k+q_j\dot{q}_k\right)\right]$$
$$-\frac{\overline{c}_{vis}}{\gamma}\left(1+\frac{1}{2}\overline{\mu}\right)\sum_{j=1}^{N_v}\sum_{k=1}^{N_v}\left(\int_0^1\tilde{\zeta}_i\tilde{\eta}_k'''\tilde{\eta}_j''\,d\alpha+\int_0^1\tilde{\zeta}_i\tilde{\eta}_k''''\tilde{\eta}_j' d\alpha\right)q_j\dot{q}_k=0,$$

$$\sum_{j=1}^{N_v}\left(\int_0^1\tilde{\eta}_i\tilde{\eta}_j d\alpha\right)\ddot{q}_j-\sqrt{\beta}\varpi_f u_{f1}\sin\left(\varpi_f\tau\right)\sum_{j=1}^{N_v}\left(\int_0^1\tilde{\eta}_i\tilde{\eta}_j' d\alpha\right)q_j+\left[u_{f0}+u_{f1}\cos\left(\varpi_f\tau\right)\right]^2\sum_{j=1}^{N_v}\left(\int_0^1\tilde{\eta}_i\tilde{\eta}_j'' d\alpha\right)q_j$$

$$-\Gamma\sum_{j=1}^{N_v}\left(\int_0^1\tilde{\eta}_i\tilde{\eta}_j'' d\alpha\right)q_j+2\sqrt{\beta}\left[u_{f0}+u_{f1}\cos\left(\varpi_f\tau\right)\right]\sum_{j=1}^{N_v}\left(\int_0^1\tilde{\eta}_i\tilde{\eta}_j' d\alpha\right)\dot{q}_j+\left(1+\bar{\mu}\right)\sum_{j=1}^{N_v}\left(\int_0^1\tilde{\eta}_i\tilde{\eta}_j'''' d\alpha\right)q_j$$

$$-\frac{\Xi_g}{\gamma}\left[\frac{3}{2\gamma}\sum_{j=1}^{N_v}\sum_{k=1}^{N_v}\sum_{l=1}^{N_v}\left(\int_0^1\tilde{\eta}_i\tilde{\eta}_k'\tilde{\eta}_j'\tilde{\eta}_l'' d\alpha\right)q_kq_jq_l+\sum_{j=1}^{N_u}\sum_{k=1}^{N_v}\left(\int_0^1\tilde{\eta}_i\tilde{\eta}_k'\tilde{\zeta}_j'' d\alpha+\int_0^1\tilde{\eta}_i\tilde{\zeta}_j'\tilde{\eta}_k'' d\alpha\right)r_jq_k\right]$$

$$+K_1\sum_{j=1}^{N_v}\left(\int_0^1\tilde{\eta}_i\tilde{\eta}_j\, d\alpha\right)q_j+K_2\sum_{j=1}^{N_v}\sum_{k=1}^{N_v}\sum_{l=1}^{N_v}\left(\int_0^1\tilde{\eta}_i\tilde{\eta}_j\tilde{\eta}_k\tilde{\eta}_l\, d\alpha\right)q_jq_kq_l$$

$$-\frac{1}{\gamma}\left[\sum_{j=1}^{N_u}\sum_{k=1}^{N_v}\left(3\int_0^1\tilde{\eta}_i\tilde{\eta}_k''\tilde{\zeta}_j''' d\alpha+\int_0^1\tilde{\eta}_i\tilde{\eta}_k'\tilde{\zeta}_j'''' d\alpha+4\int_0^1\tilde{\eta}_i\tilde{\eta}_k'''\tilde{\zeta}_j'' d\alpha+2\int_0^1\tilde{\eta}_i\tilde{\zeta}_j'\tilde{\eta}_k'''' d\alpha\right)r_jq_k\right.$$

$$\left.+\frac{1}{\gamma}\sum_{j=1}^{N_v}\sum_{k=1}^{N_v}\sum_{l=1}^{N_v}\left(2\int_0^1\tilde{\eta}_i\tilde{\eta}_k''\tilde{\eta}_j''\tilde{\eta}_l'' d\alpha+2\int_0^1\tilde{\eta}_i\tilde{\eta}_k'\tilde{\eta}_j'\tilde{\eta}_l'''' d\alpha+8\int_0^1\tilde{\eta}_i\tilde{\eta}_k''\tilde{\eta}_j'\tilde{\eta}_l''' d\alpha\right)q_jq_kq_l\right]$$

$$-\frac{\bar{\mu}}{4\gamma}\left[\sum_{j=1}^{N_u}\sum_{k=1}^{N_v}\left(6\int_0^1\tilde{\eta}_i\tilde{\eta}_k''\tilde{\zeta}_j''' d\alpha+2\int_0^1\tilde{\eta}_i\tilde{\eta}_k'\tilde{\zeta}_j'''' d\alpha+8\int_0^1\tilde{\eta}_i\tilde{\eta}_k'''\tilde{\zeta}_j'' d\alpha+4\int_0^1\tilde{\eta}_i\tilde{\zeta}_j'\tilde{\eta}_k'''' d\alpha\right)r_jq_k\right.$$

$$\left.+\frac{1}{\gamma}\sum_{j=1}^{N_v}\sum_{k=1}^{N_v}\sum_{l=1}^{N_v}\left(5\int_0^1\tilde{\eta}_i\tilde{\eta}_k''\tilde{\eta}_j''\tilde{\eta}_l'' d\alpha+5\int_0^1\tilde{\eta}_i\tilde{\eta}_k'\tilde{\eta}_j'\tilde{\eta}_l'''' d\alpha+20\int_0^1\tilde{\eta}_i\tilde{\eta}_k''\tilde{\eta}_j'\tilde{\eta}_l''' d\alpha\right)q_jq_kq_l\right]$$

$$-\frac{1}{4}\frac{\bar{\mu}}{\Xi_g\gamma^2}\sum_{j=1}^{N_v}\sum_{k=1}^{N_v}\sum_{l=1}^{N_v}\left(3\int_0^1\tilde{\eta}_i\tilde{\eta}_k'''\tilde{\eta}_j''\tilde{\eta}_l''' d\alpha+6\int_0^1\tilde{\eta}_i\tilde{\eta}_k''\tilde{\eta}_j'\tilde{\eta}_l^{(5)} d\alpha+10\int_0^1\tilde{\eta}_i\tilde{\eta}_k'''\tilde{\eta}_j'\tilde{\eta}_l'''' d\alpha\right.$$

$$\left.+\int_0^1\tilde{\eta}_i\tilde{\eta}_k'\tilde{\eta}_j'\tilde{\eta}_l^{(6)} d\alpha+4\int_0^1\tilde{\eta}_i\tilde{\eta}_k''\tilde{\eta}_j''\tilde{\eta}_l'''' d\alpha\right)q_jq_kq_l$$

$$-\frac{\bar{c}_{vis}\Xi_g}{\gamma}\left[\frac{1}{\gamma}\sum_{j=1}^{N_v}\sum_{k=1}^{N_v}\sum_{l=1}^{N_v}\left(\int_0^1\tilde{\eta}_i\tilde{\eta}_k'\tilde{\eta}_j'\tilde{\eta}_l'' d\alpha\right)\left(2q_j\dot{q}_kq_l+q_jq_k\dot{q}_l\right)+\sum_{j=1}^{N_u}\sum_{k=1}^{N_v}\left(\int_0^1\tilde{\eta}_i\tilde{\eta}_k'\tilde{\zeta}_j'' d\alpha+\int_0^1\tilde{\eta}_i\tilde{\eta}_k''\tilde{\zeta}_j' d\alpha\right)\dot{r}_jq_k\right]$$

$$+\bar{c}_{vis}\left(1+\bar{\mu}\right)\sum_{j=1}^{N_v}\left(\int_0^1\tilde{\eta}_i\tilde{\eta}_j'''' d\alpha\right)\dot{q}_j-\frac{\bar{c}_{vis}}{\gamma}\left[\sum_{j=1}^{N_u}\sum_{k=1}^{N_v}\left(3\int_0^1\tilde{\eta}_i\tilde{\zeta}_j'''\tilde{\eta}_k''\, d\alpha+\int_0^1\tilde{\eta}_i\tilde{\eta}_k'\tilde{\zeta}_j'''' d\alpha\right)\left(\dot{r}_jq_k+r_j\dot{q}_k\right)\right.$$

$$+\sum_{j=1}^{N_u}\sum_{k=1}^{N_v}\left(\int_0^1\tilde{\eta}_i\tilde{\zeta}_j''\tilde{\eta}_k''' d\alpha\right)\left(3\dot{r}_jq_k+4r_j\dot{q}_k\right)+\sum_{j=1}^{N_u}\sum_{k=1}^{N_v}\left(\int_0^1\tilde{\eta}_i\tilde{\zeta}_j'\tilde{\eta}_k'''' d\alpha\right)\left(\dot{r}_jq_k+2r_j\dot{q}_k\right)$$

$$\left.+\frac{1}{\gamma}\sum_{j=1}^{N_v}\sum_{k=1}^{N_v}\sum_{l=1}^{N_v}\left(\int_0^1\tilde{\eta}_i\tilde{\eta}_j'\tilde{\eta}_k''\tilde{\eta}_l''' d\alpha\right)\left(6\dot{q}_jq_kq_l+6q_j\dot{q}_kq_l+8q_jq_k\dot{q}_l\right)\right.$$

$$+\frac{2}{\gamma}\sum_{j=1}^{N_v}\sum_{k=1}^{N_v}\sum_{l=1}^{N_v}\left(\int_0^1\tilde{\eta}_i\tilde{\eta}_j'\tilde{\eta}_k'\tilde{\eta}_l''''d\alpha\right)\left(\dot{q}_jq_kq_l+q_jq_k\dot{q}_l\right)+\frac{6}{\gamma}\sum_{j=1}^{N_v}\sum_{k=1}^{N_v}\sum_{l=1}^{N_v}\left(\int_0^1\tilde{\eta}_i\tilde{\eta}_k''\tilde{\eta}_j''\tilde{\eta}_l''d\alpha\right)q_jq_k\dot{q}_l\Bigg]$$

$$-\frac{\overline{\mu c}_{vis}}{4\gamma}\Bigg[\sum_{j=1}^{N_u}\sum_{k=1}^{N_v}\left(2\int_0^1\tilde{\eta}_i\tilde{\eta}_k'\tilde{\zeta}_j''''d\alpha+6\int_0^1\tilde{\eta}_i\tilde{\eta}_k''\tilde{\zeta}_j'''d\alpha\right)\left(q_k\dot{r}_j+r_j\dot{q}_k\right)$$

$$+\sum_{j=1}^{N_u}\sum_{k=1}^{N_v}\left(\int_0^1\tilde{\eta}_i\tilde{\zeta}_j''\tilde{\eta}_k'''d\alpha\right)\left(6\dot{r}_jq_k+8r_j\dot{q}_k\right)+\sum_{j=1}^{N_u}\sum_{k=1}^{N_v}\left(\int_0^1\tilde{\eta}_i\tilde{\eta}_k''''\tilde{\zeta}_j'd\alpha\right)\left(2\dot{r}_jq_k+4r_j\dot{q}_k\right)$$

$$+\frac{1}{\gamma}\sum_{j=1}^{N_v}\sum_{k=1}^{N_v}\sum_{l=1}^{N_v}\left(\int_0^1\tilde{\eta}_i\tilde{\eta}_j'\tilde{\eta}_k''\tilde{\eta}_l'''d\alpha\right)\left(17\dot{q}_jq_kq_l+15q_j\dot{q}_kq_l+20q_jq_k\dot{q}_l\right)+$$

$$\frac{5}{\gamma}\sum_{j=1}^{N_v}\sum_{k=1}^{N_v}\sum_{l=1}^{N_v}\left(\int_0^1\tilde{\eta}_i\tilde{\eta}_j'\tilde{\eta}_k'\tilde{\eta}_l''''d\alpha\right)\left(\dot{q}_jq_kq_l+q_jq_k\dot{q}_l\right)+\frac{16}{\gamma}\sum_{j=1}^{N_v}\sum_{k=1}^{N_v}\sum_{l=1}^{N_v}\left(\int_0^1\tilde{\eta}_i\tilde{\eta}_j''\tilde{\eta}_k''\tilde{\eta}_l''d\alpha\right)q_jq_k\dot{q}_l\Bigg]$$

$$-\frac{\overline{\mu c}_{vis}}{4\Xi_g\gamma^2}\Bigg[\sum_{j=1}^{N_v}\sum_{k=1}^{N_v}\sum_{l=1}^{N_v}\left(\int_0^1\tilde{\eta}_i\tilde{\eta}_k''\tilde{\eta}_j'\tilde{\eta}_l^{(5)}d\alpha\right)\left(\dot{q}_jq_kq_l+5q_j\dot{q}_kq_l+6q_jq_k\dot{q}_l\right)$$

$$+\sum_{j=1}^{N_v}\sum_{k=1}^{N_v}\sum_{l=1}^{N_v}\left(\int_0^1\tilde{\eta}_i\tilde{\eta}_j'\tilde{\eta}_k'\tilde{\eta}_l^{(6)}d\alpha\right)\left(q_j\dot{q}_kq_l+q_jq_k\dot{q}_l\right)+6\sum_{j=1}^{N_v}\sum_{k=1}^{N_v}\sum_{l=1}^{N_v}\left(\int_0^1\tilde{\eta}_i\tilde{\eta}_j''\tilde{\eta}_k'''\tilde{\eta}_l'''d\alpha\right)q_jq_k\dot{q}_l$$

$$+4\sum_{j=1}^{N_v}\sum_{k=1}^{N_v}\sum_{l=1}^{N_v}\left(\int_0^1\tilde{\eta}_i\tilde{\eta}_j''\tilde{\eta}_k''\tilde{\eta}_l''''d\alpha\right)\left(q_j\dot{q}_kq_l+q_jq_k\dot{q}_l\right)$$

$$+10\sum_{j=1}^{N_v}\sum_{k=1}^{N_v}\sum_{l=1}^{N_v}\left(\int_0^1\tilde{\eta}_i\tilde{\eta}_j'\tilde{\eta}_k'''\tilde{\eta}_l''''d\alpha\right)\left(q_j\dot{q}_kq_l+q_jq_k\dot{q}_l\right)\Bigg]=0,\qquad i=1,2,...,N_v.$$

(20)

Assuming a viscoelastic microscale tube with clamped-clamped boundary conditions, and using the appropriate shape functions for this type of boundary conditions, the bifurcation characteristics can be determined on the basis of a continuation approach. In the present paper, 16 shape functions (8 for axial and 8 for transverse displacements) are taken into consideration in all numerical calculations for the displacements along both *x* and *z* directions.

3. Numerical results

A viscoelastic microscale tube with internal radius R_i=17.5 μm, external radius R_o=25 μm, and length-to-radius L/R_o = 280 is considered in this section for numerical results. The microtube Poisson's ratio and Young's modulus are as ν=0.38 and E=1.44 GPa, respectively.

In addition, the mass density of the microstructure and the microfluid are taken as ρ_p=1220 kg/m^3, and ρ_f =1000 kg/m^3, respectively. The non-dimensional parameters of the microscale fluid-structure system are obtained as Ξ_g =2.1047×10^5, β=0.4406, γ =140, and $\bar{\mu}$ =0.4821. For all cases, the non-dimensional longitudinal pretention, viscosity constant and spring constants are set to Γ =6.0, $\bar{c}_{vis}$ =0.0003, and (K_1,K_2)=(80.0,80.0), respectively. The ratio of the frequency of the fluid speed to the first natural frequency is assumed as ϖ_f/ω_1=2.0. The dimensionless critical fluid speed of the above-described microsystem associated with divergence is determined as 8.4001. It should be noted that in this section bifurcation diagrams are plotted for transverse and longitudinal motions at α =0.45, instead of 0.5, to ensure all modes (symmetric and asymmetric) have non-zero value and contribute to the response of the system.

Figure 2 indicates the bifurcation diagrams of Poincaré sections (BDPS) of the viscoelastic microtube conveying pulsatile flow for displacements along both *x* and *z* directions. The dimensionless mean value of the fluid speed is assumed as u_{f0}=8.0 which means that the viscoelastic microsystem is in the subcritical regime. The dimensionless first natural frequency of the viscoelastic microscale fluid-structure system is determined as ω_1= 7.67. It is observed that when the amplitude of fluid speed variations is very small (u_{f1}<0.02), the nonlinear transverse motion of the viscoelastic microtube is of a period-1 type. Beyond that a period-2 motion is observed for the microtube until point u_{f1}=0.81 where the motion type is period-6. Then the nonlinear dynamic behaviour fluctuates between period-2 and period-6 motions until u_{f1}=0.89 where only a period-2 motion is observed. Beyond this point, various motion types in the form of period-*k* (*k*=1, 2, 3, 4, 6 and 9) are found for the transverse deflection of the viscoelastic fluid-structure microsystem. It is worth mentioning that no

complex behaviour such as chaos is found for the transverse motion in the subcritical regime. From Fig. 2, it is also found that the axial motion is of a period-1 type until u_{f1}=0.81 in which it begins to fluctuate between a period-3 and period-1 type. From u_{f1}=0.89 to u_{f1}=1.12, a period-1 axial motion is observed, except point u_{f1}=0.915 where the system experiences a period-9 axial motion. From u_{f1}=1.13 to u_{f1}=2, various simple motion types such as period-1, period-2 and period-3 are found for the axial displacement. However, there is no sign of a complex behaviour such as chaos for the axial motion. More details of the periodic motion of the pulsatile-fluid-conveying microtube of Fig. 2 at u_{f1}=1.200 in the subcritical regime is given in Figure 3. The time histories of motions along both *x* and *z* directions, fast Fourier transforms (FFTs) and the phase-plane portraits are illustrated in the figure. At this point (u_{f1}=1.200), both longitudinal and transverse motions are of a period-1 type.

The BDPS for the viscoelastic microtube conveying pulsatile fluid with mean speed of u_{f0}=8.3 (i.e. in the subcritical regime) for both motions along the transverse and axial directions is plotted in Fig. 4; compared to the case of Fig. 2, this mean speed is closer to the critical one. The fundamental natural frequency is calculated as ω_1= 3.78. For the small values of the speed amplitude, the transverse motion is of a perid-2 type while the microscale tube experiences a period-1 motion along the axial axes. As the amplitude of the fluid speed variations increases, the microtube undergoes various types of transverse motions including period-6, period-4, period-3, period-1 and chaos. Moreover, different motion types such as period-2, priod-3, period-4 and chaos are observed for the axial displacements. From Fig. 4, eight different chaotic regions are seen for both the longitudinal and transverse motions of the microtube. The first chaotic region begins at u_{f1}=0.562 and ends at u_{f1}=0.658 while the last one starts at u_{f1}=1.822 and ends at u_{f1}=2.022. By comparing the BDPS of Fig. 2 with that

of Fig. 4, it is found that a small increase in the mean speed of the pulsatile flow in the vicinity of the critical speed in the subcritical regime notably increases the complexity of the nonlinear dynamic behaviour. More details of the motion of the microtube of Fig. 4 at u_{f1}=1.190 and u_{f1}=1.138 are given in Figs. 5 and 6, respectively. It is found that the motion of the microtube is of a period-4 type at u_{f1}=1.190 while a complex chaotic motion is observed at u_{f1}=1.138 for the microtube.

Figure 7 illustrates the BDPS for the viscoelastic microtube conveying pulsatile fluid with mean speed of u_{f0}=8.5 which belongs to the supercritical regime. The fundamental natural frequency of the viscoelastic microtube is determined as ω_1= 5.29. It is observed that the type of both transverse and axial motions is period-2 for small values of the velocity amplitude. By further increasing the fluctuation amplitude of the pulsatile flow, a variety of different motions such as period-1, period-2, period-6 and chaos is observed for the microsystem. For instance, the details of the motion of the viscoelastic microscale tube of Fig. 7 at u_{f1}=1.106 are shown in Fig. 8. It can be seen that the nonlinear bifurcation behaviour is highly chaotic at this point. For comparison purposes, the BDPS for the viscoelastic microtube conveying pulsatile flow for u_{f0}=9.0 is indicated in Fig. 9, but this time a bit more farther from the critical speed (compared to the case of Fig. 7). The first non-dimensional natural frequency of the microscale fluid-structure system is obtained as ω_1= 12.71 for this case. The motion type along each axis varies significantly with increasing the amplitude of the variations of the fluid speed from u_{f0}=0 to u_{f0}=2.022. However, no sign of chaos is observed for the viscoelastic microtube in this region. Furthermore, by comparing Fig. 9 with Fig. 7, it can be concluded that a slight increase in the mean speed of the pulsatile flow in the supercritical regime can eliminate the chaotic motion.

4. Conclusions

The large-amplitude oscillations of a viscoelastic microtube conveying pulsatile flow has been investigated. The microscale tube was embedded in a nonlinear spring bed. The coupled time-dependent nonlinear equations were derived via the assistance of the MCST in conjunction with the Euler-Bernoulli and Kelvin-Voigt models as well as Hamilton's principle. Galerkin's approach, as a discretisation method, and a direct time-integration approach, as a solution technique, were also employed to construct the BDPS for the microfluid-structure microscale system.

It was concluded that both the mean value and the amplitude of the speed of the pulsatile flow have a vital role to play in the bifurcation response. When the mean speed of the pulsatile fluid is sufficiently lower than the critical speed in the subcritical regime and the speed amplitude is very small, the nonlinear motion of the microtube is of a period-1 type and there is no chaos in the motion of the viscoelastic microtube. For a larger mean speed close to the critical speed, but still in the subcritical regime, the microtube experiences various types of motions including period-6, period-4, period-3, period-1 and chaos. In fact, a slight increase in the mean fluid speed even in the subcritical regime can cause a huge difference in the bifurcation response of viscoelastic microscale tubes containing pulsatile flow. The type of both motions along the axial and transverse directions is period-2 when the fluctuation amplitude of the pulsatile flow is very small and the mean speed is a bit larger than the critical one. By further increasing the fluctuation amplitude, different motions such as period-1, period-2, period-6 and chaos were observed for the microtube. However, a sufficient increase in the mean speed can completely remove the chaotic behaviour in the supercritical regime.

References

[1] M.E. Warkiani, G. Guan, K.B. Luan, W.C. Lee, A.A.S. Bhagat, P.K. Chaudhuri, D.S.-W. Tan, W.T. Lim, S.C. Lee, P.C. Chen, Slanted spiral microfluidics for the ultra-fast, label-free isolation of circulating tumor cells, Lab on a Chip, 14 (2014) 128-137.

[2] D. Alveringh, R.J. Wiegerink, J.C. Lötters, Integrated pressure sensing using capacitive coriolis mass flow sensors, Journal of Microelectromechanical Systems, 26 (2017) 653-661.

[3] M. Şimşek, Dynamic analysis of an embedded microbeam carrying a moving microparticle based on the modified couple stress theory, International Journal of Engineering Science, 48 (2010) 1721-1732.

[4] M. Aydogdu, A nonlocal rod model for axial vibration of double-walled carbon nanotubes including axial van der Waals force effects, Journal of Vibration and Control, 21 (2015) 3132-3154.

[5] T. Murmu, S. Adhikari, C. Wang, Torsional vibration of carbon nanotube–buckyball systems based on nonlocal elasticity theory, Physica E: Low-dimensional Systems and Nanostructures, 43 (2011) 1276-1280.

[6] L.-L. Ke, Y.-S. Wang, J. Yang, S. Kitipornchai, Free vibration of size-dependent Mindlin microplates based on the modified couple stress theory, Journal of Sound and Vibration, 331 (2012) 94-106.

[7] A. Hadi, M.Z. Nejad, M. Hosseini, Vibrations of three-dimensionally graded nanobeams, International Journal of Engineering Science, 128 (2018) 12-23.

[8] L. Wang, Size-dependent vibration characteristics of fluid-conveying microtubes, Journal of Fluids and Structures, 26 (2010) 675-684.

[9] S. Kural, E. Özkaya, Size-dependent vibrations of a micro beam conveying fluid and resting on an elastic foundation, Journal of Vibration and Control, 23 (2017) 1106-1114.

[10] M. Hosseini, R. Bahaadini, Size dependent stability analysis of cantilever micro-pipes conveying fluid based on modified strain gradient theory, International Journal of Engineering Science, 101 (2016) 1-13.

[11] A.M. Dehrouyeh-Semnani, M. Nikkhah-Bahrami, M.R.H. Yazdi, On nonlinear vibrations of micropipes conveying fluid, International Journal of Engineering Science, 117 (2017) 20-33.

[12] R. Bahaadini, M. Hosseini, Nonlocal divergence and flutter instability analysis of embedded fluid-conveying carbon nanotube under magnetic field, Microfluidics and Nanofluidics, 20 (2016) 108.

[13] R. Ansari, A. Norouzzadeh, R. Gholami, M.F. Shojaei, M. Darabi, Geometrically nonlinear free vibration and instability of fluid-conveying nanoscale pipes including surface stress effects, Microfluidics and Nanofluidics, 20 (2016) 28.

[14] H. Liu, Z. Lv, Q. Li, Flexural wave propagation in fluid-conveying carbon nanotubes with system uncertainties, Microfluidics and Nanofluidics, 21 (2017) 140.

[15] H. Askari, E. Esmailzadeh, Forced vibration of fluid conveying carbon nanotubes considering thermal effect and nonlinear foundations, Composites Part B: Engineering, 113 (2017) 31-43.

[16] A.M. Dehrouyeh-Semnani, M. Nikkhah-Bahrami, M.R.H. Yazdi, On nonlinear stability of fluid-conveying imperfect micropipes, International Journal of Engineering Science, 120 (2017) 254-271.

[17] A. Setoodeh, S. Afrahim, Nonlinear dynamic analysis of FG micro-pipes conveying fluid based on strain gradient theory, Composite Structures, 116 (2014) 128-135.

[18] M. Tang, Q. Ni, L. Wang, Y. Luo, Y. Wang, Nonlinear modeling and size-dependent vibration analysis of curved microtubes conveying fluid based on modified couple stress theory, International Journal of Engineering Science, 84 (2014) 1-10.

[19] W. Xia, L. Wang, Microfluid-induced vibration and stability of structures modeled as microscale pipes conveying fluid based on non-classical Timoshenko beam theory, Microfluidics and Nanofluidics, 9 (2010) 955-962.

[20] L. Li, Y. Hu, X. Li, L. Ling, Size-dependent effects on critical flow velocity of fluid-conveying microtubes via nonlocal strain gradient theory, Microfluidics and Nanofluidics, 20 (2016) 76.

[21] M. Hosseini, A.Z.B. Maryam, R. Bahaadini, Forced vibrations of fluid-conveyed double piezoelectric functionally graded micropipes subjected to moving load, Microfluidics and Nanofluidics, 21 (2017) 134.

Figures

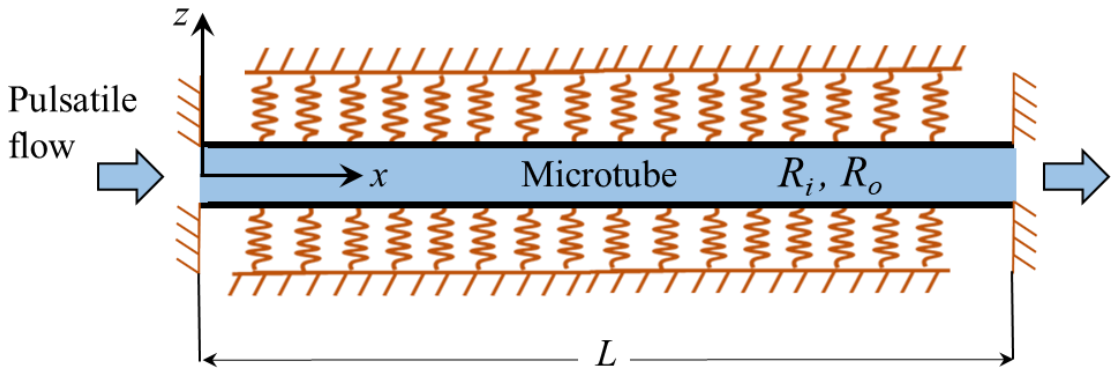

Figure 1: A pulsatile-fluid-conveying viscoelastic microtube embedded in an elastic medium.

(a)

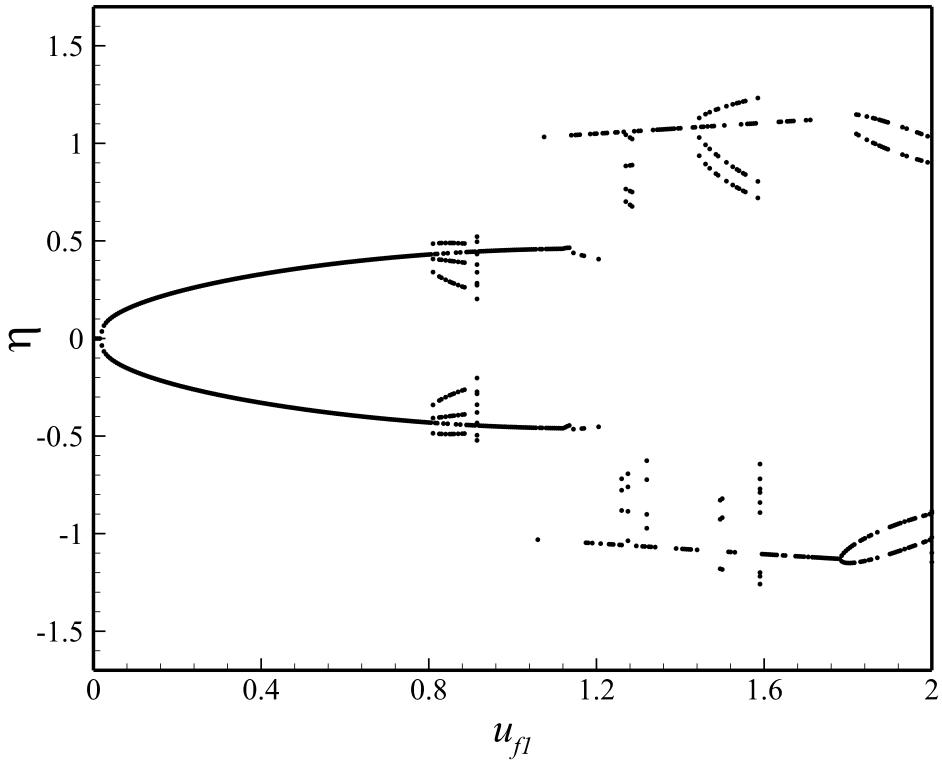

(b)

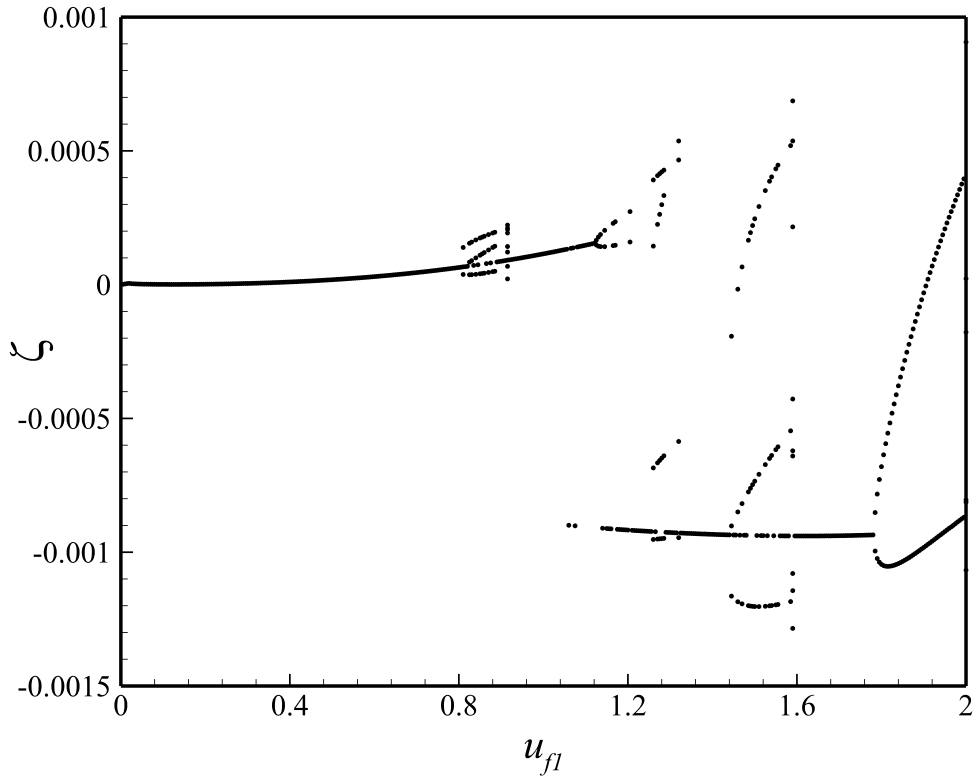

Figure 2: BDPS for the viscoelastic microtube conveying pulsatile flow: (a, b) the transverse motion and longitudinal motions for u_{f0}=8.0.

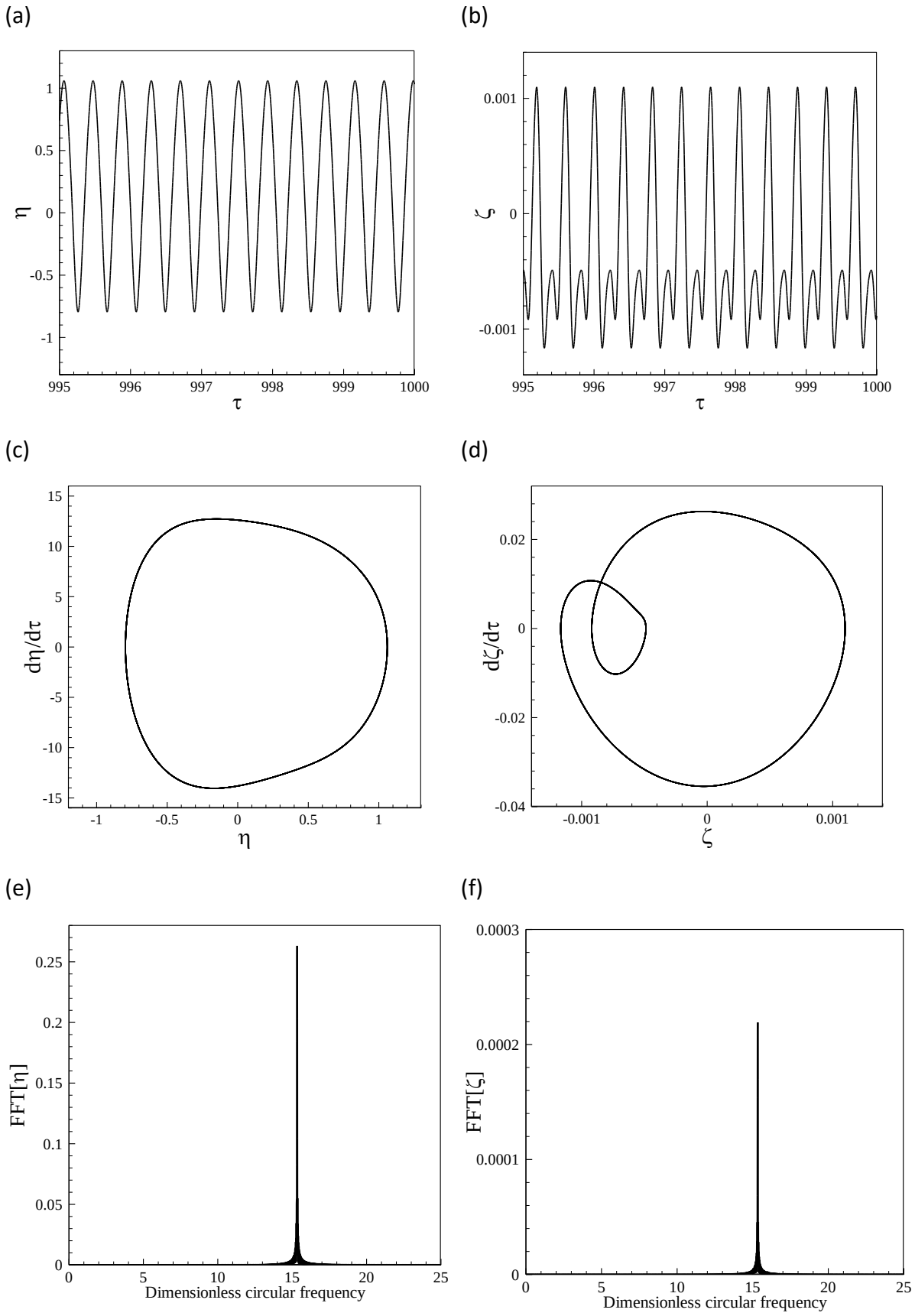

Figure 3: Details of the periodic motion of the system of Fig. 2 at u_{f1}=1.200: (a, b) the time histories of transverse and longitudinal motions, respectively; (c, d) the phase-plane portrait of transverse and longitudinal motions, respectively; (e, f) FFTs of transverse and longitudinal motions, respectively.

(a)

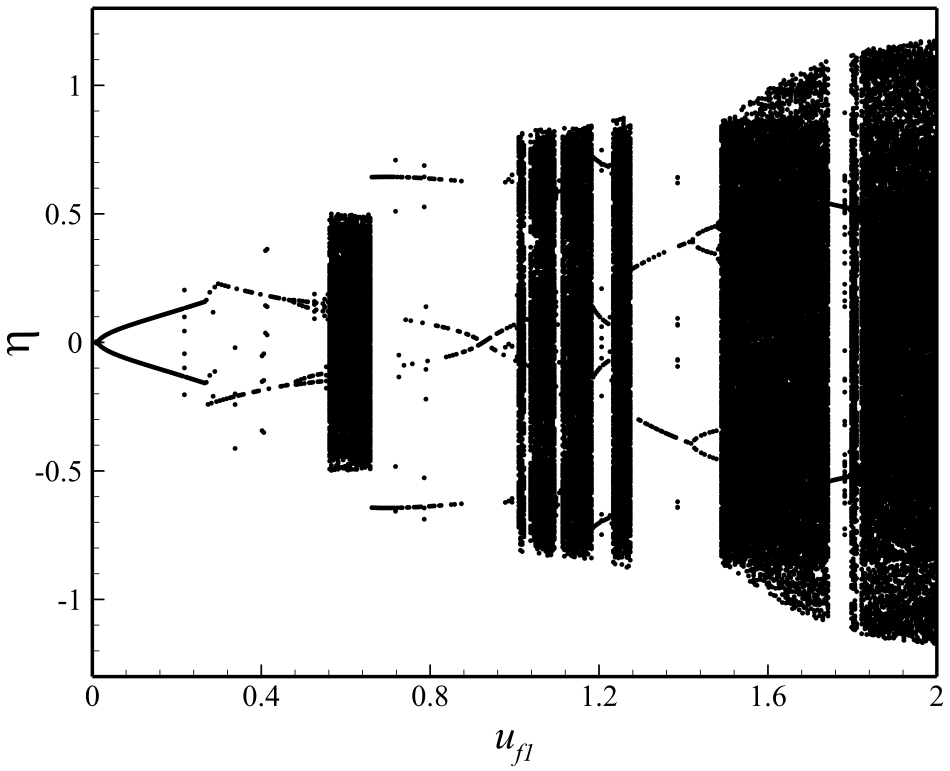

(b)

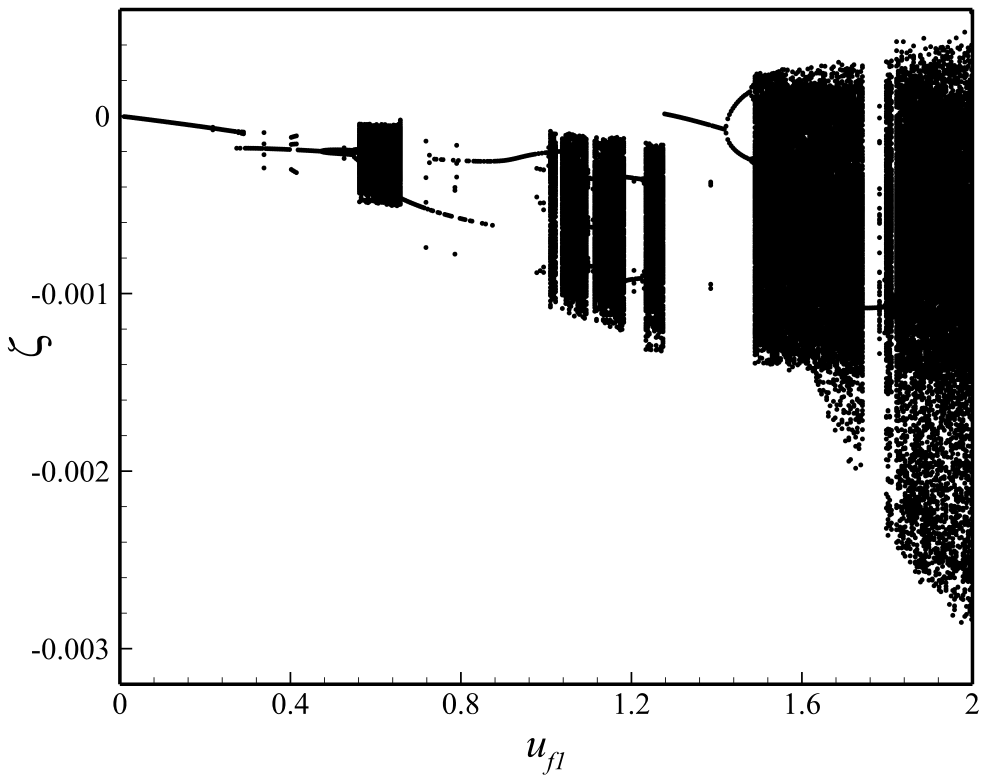

Figure 4: BDPS for the viscoelastic microtube conveying pulsatile flow: (a, b) the transverse motion and longitudinal motions for u_{f0}=8.3.

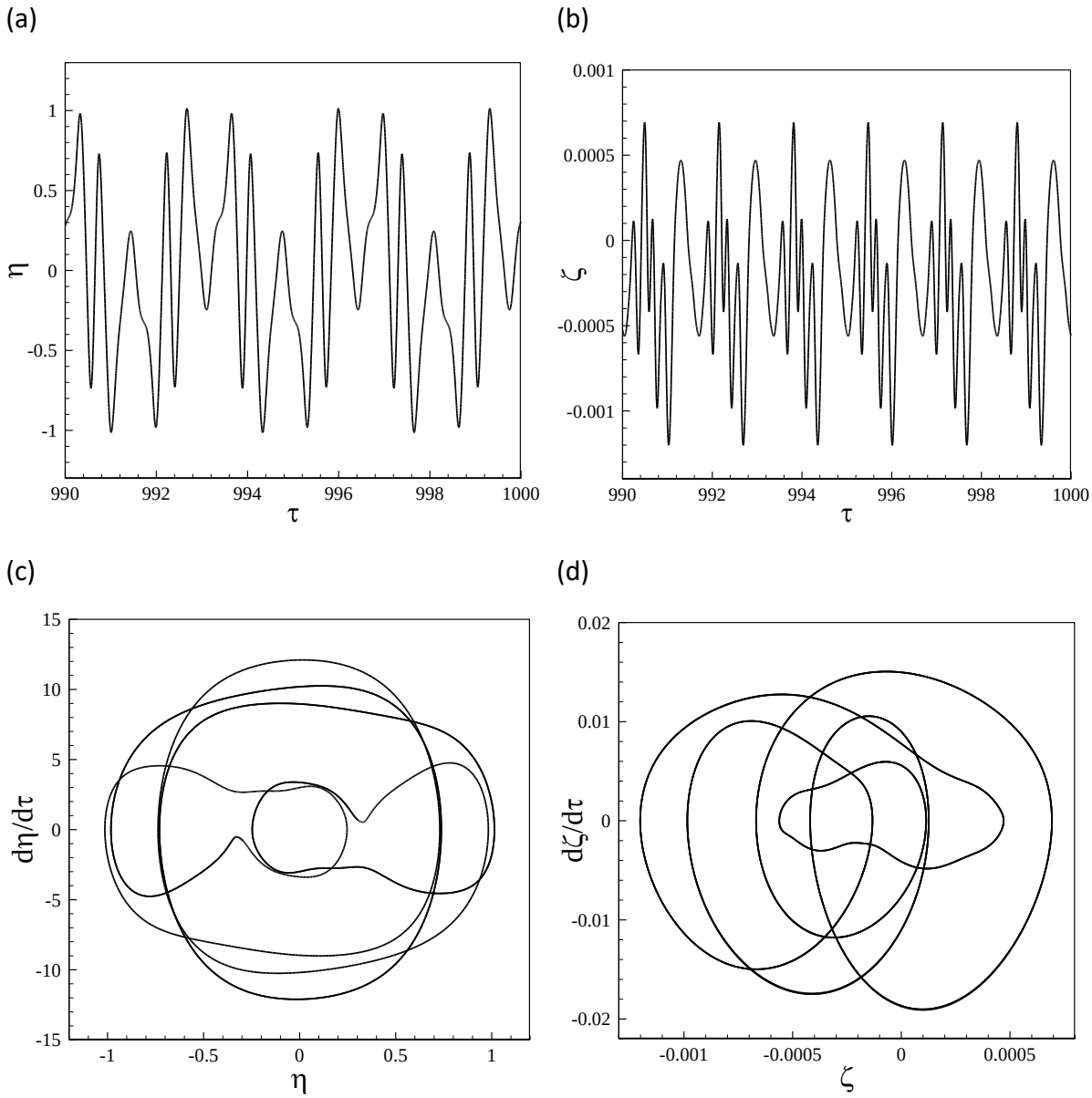

Figure 5: Details of the period-4 motion of the system of Fig. 4 at u_{f1}=1.190: (a, b) the time histories of transverse and longitudinal motions, respectively; (c, d) the phase-plane portrait of transverse and longitudinal motions, respectively.

(a)

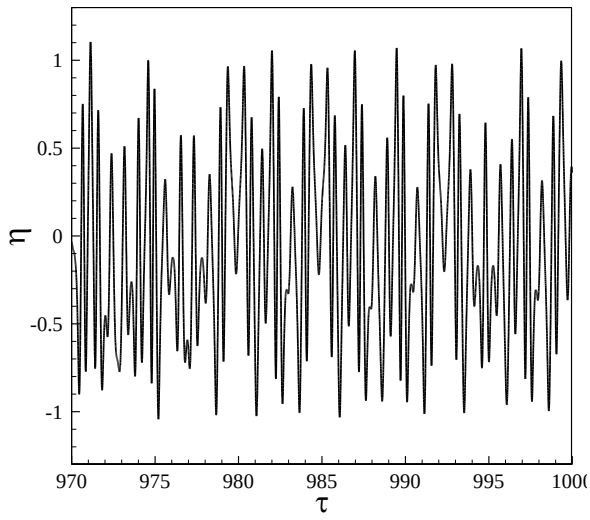

(b)

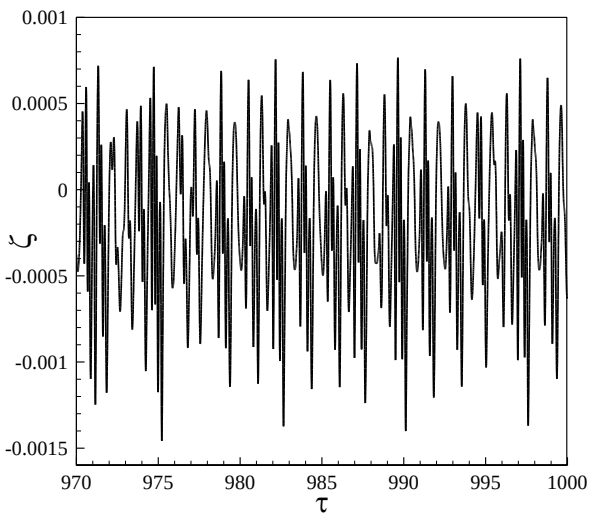

(c)

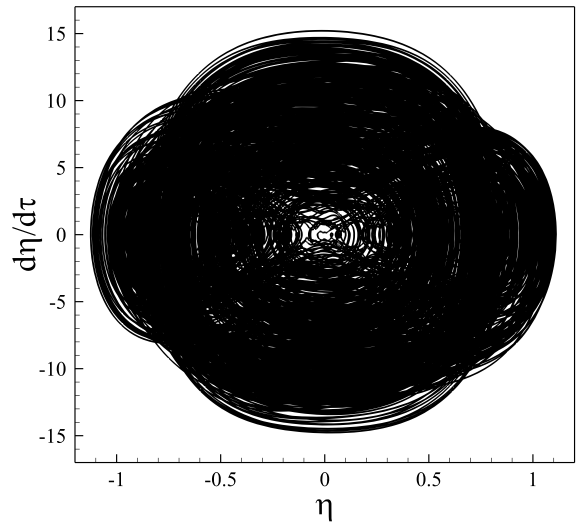

(d)

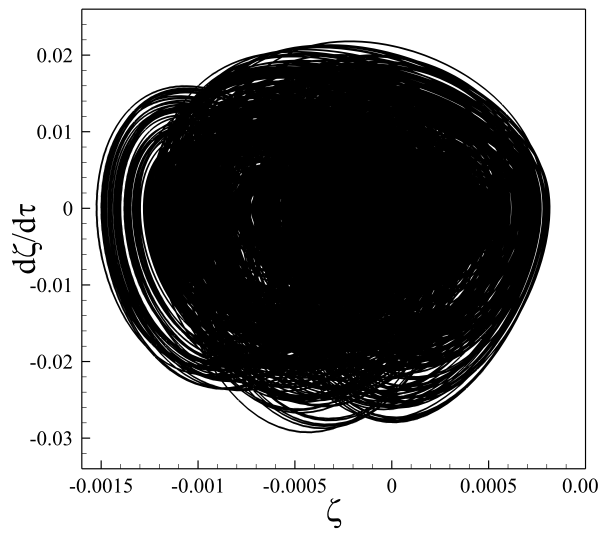

(e)

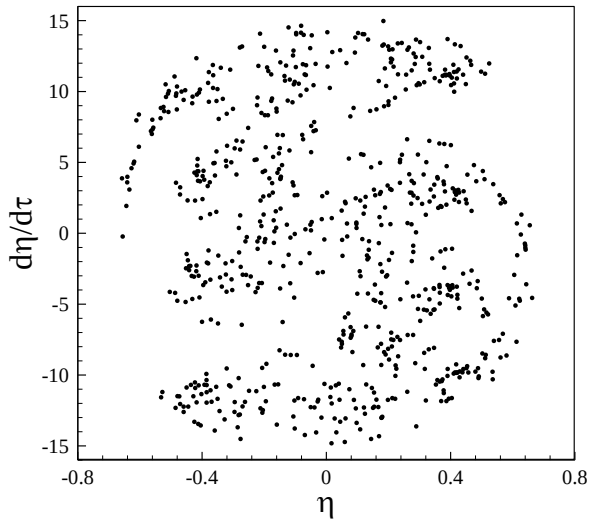

(f)

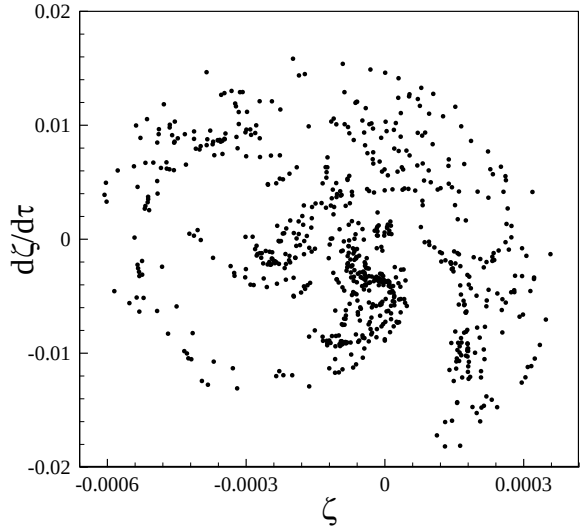

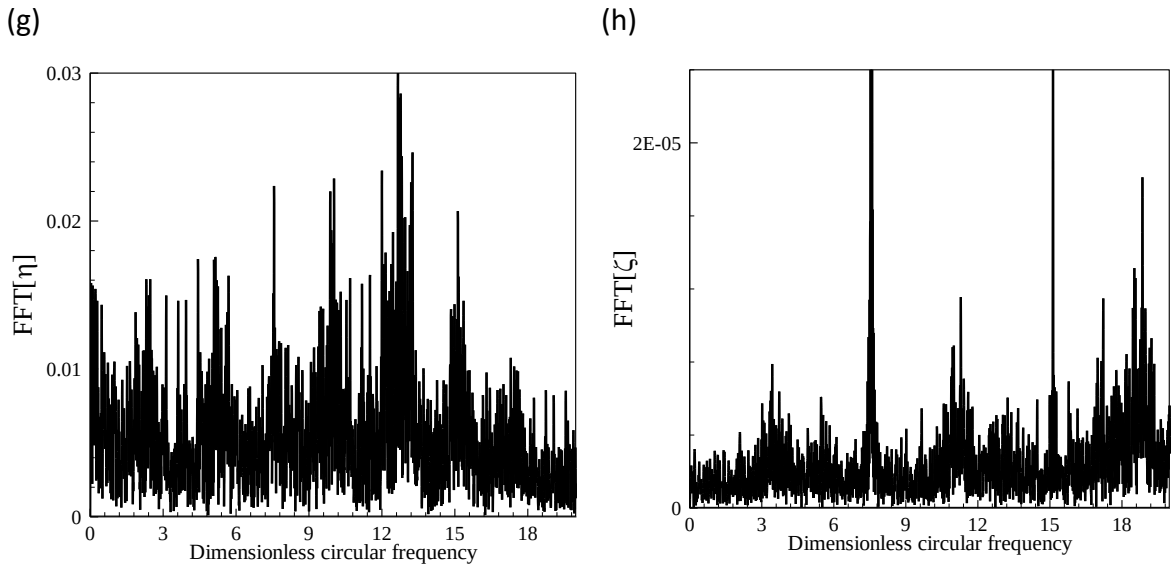

Figure 6: Details of the chaotic motion of the system of Fig. 4 at u_{f1}=1.138: (a, b) the time histories of transverse and longitudinal motions, respectively; (c, d) the phase-plane portrait of transverse and longitudinal motions, respectively; (e, f) Poincaré sections of transverse and longitudinal motions, respectively; (g, h) FFTs of transverse and longitudinal motions, respectively.

(a)

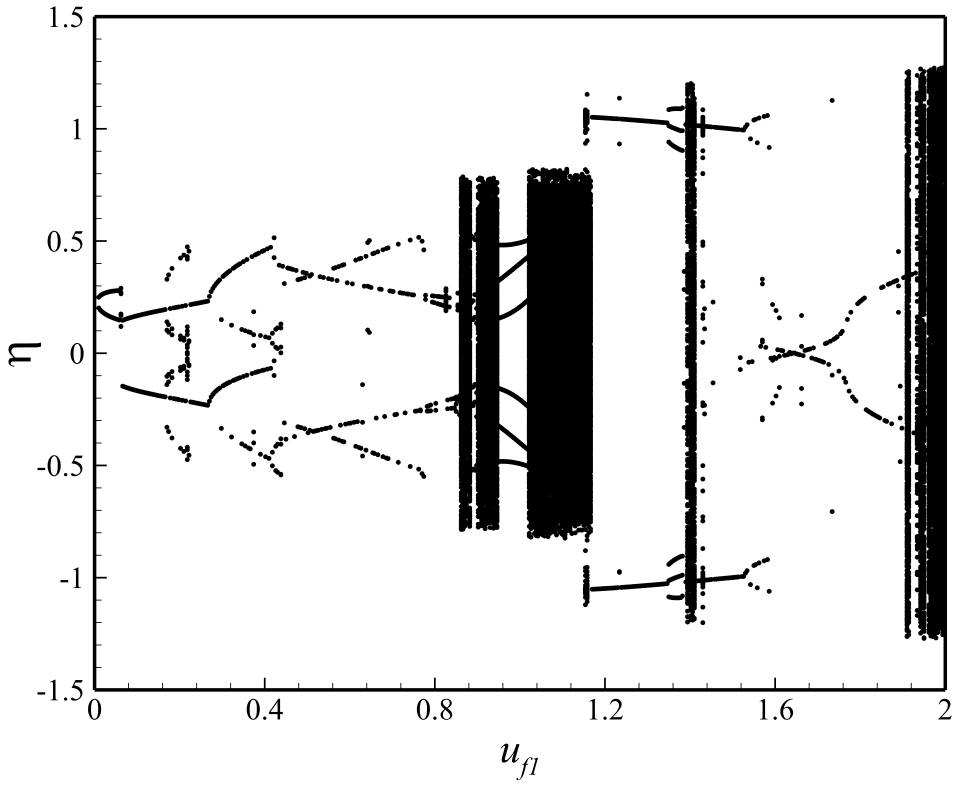

(b)

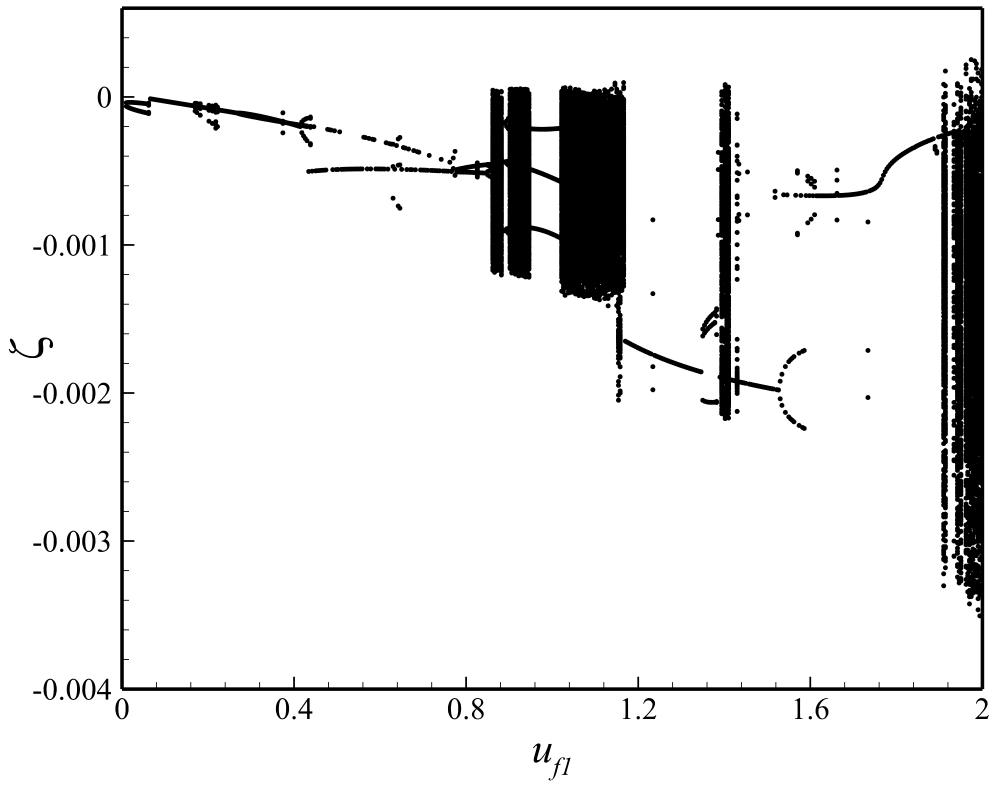

Figure 7: BDPS for the viscoelastic microtube conveying pulsatile flow: (a, b) the transverse motion and longitudinal motions for u_{f0}=8.5.

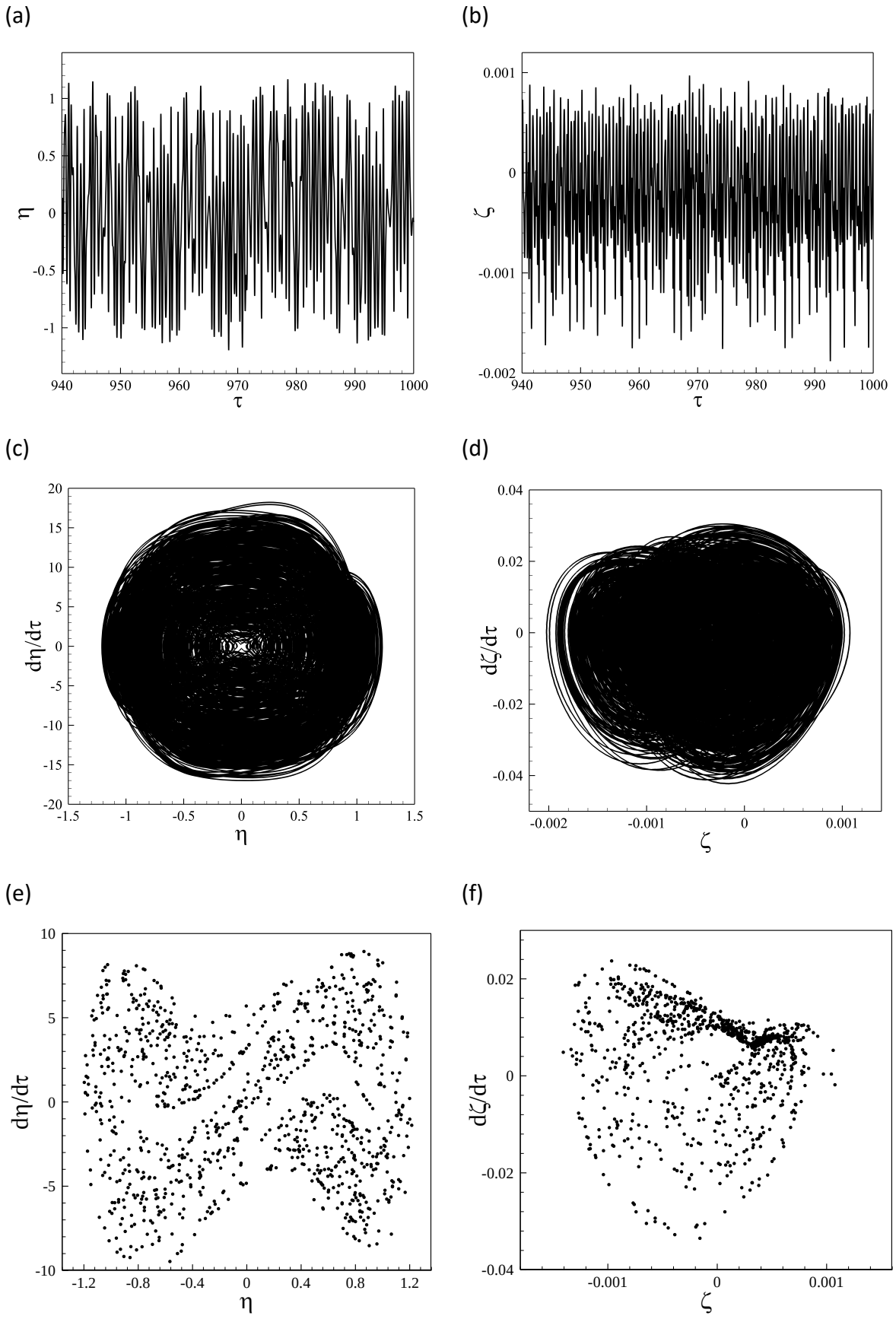

Figure 8: Details of the chaotic motion of the system of Fig. 7 at u_{f1}=1.106: (a, b) the time histories of transverse and longitudinal motions, respectively; (c, d) the phase-plane portrait of transverse and longitudinal motions, respectively; (e, f) Poincaré sections of transverse and longitudinal motions, respectively.

(a)

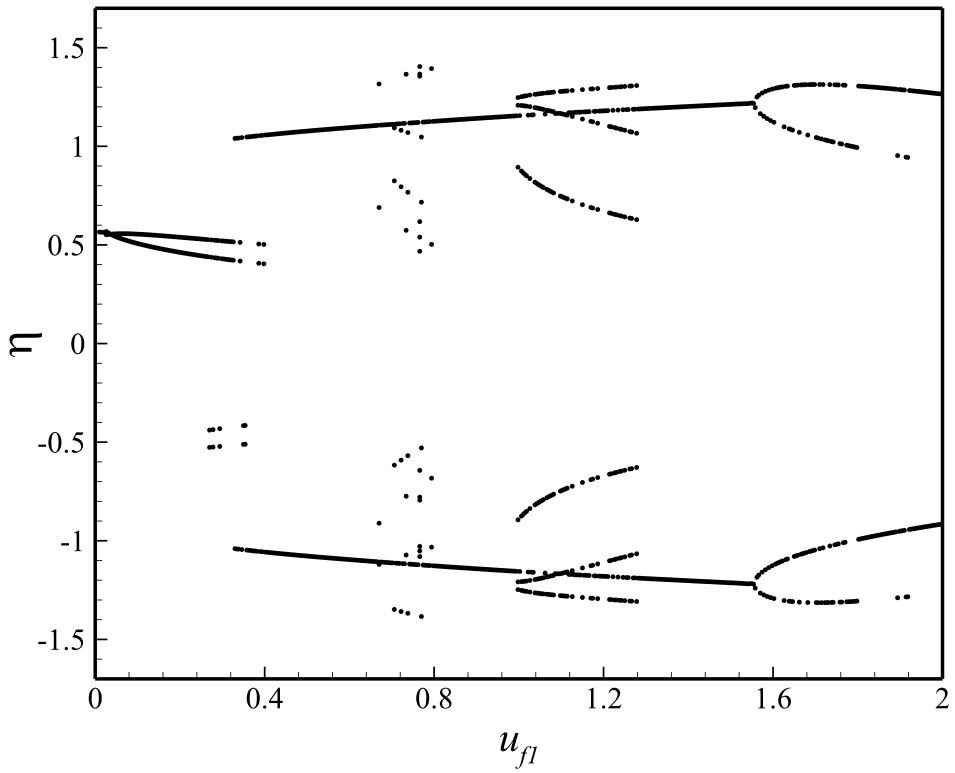

(b)

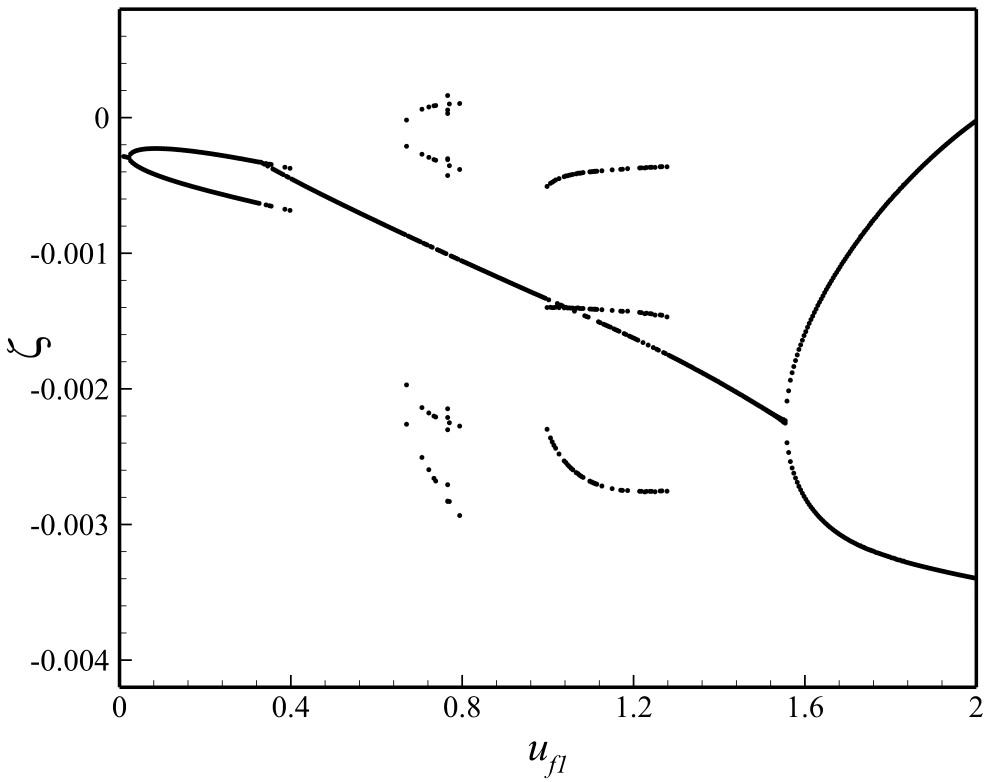

Figure 9: BDPS for the viscoelastic microtube conveying pulsatile flow: (a, b) the transverse motion and longitudinal motions for u_{f0}=9.0.